

# 1 Geophysical downhole logging analysis within the shallow depth ICDP

## 2 STAR drilling project (Central Italy)

3 Paola Montone<sup>1</sup> \*, Simona Pierdominici<sup>2</sup>, M. Teresa Mariucci<sup>1</sup>, Francesco Mirabella<sup>3</sup>, Marco Urbani<sup>3</sup>,  
4 Assel Akimbekova<sup>3</sup>, Lauro Chiaraluce<sup>1</sup>, Wade Johnson<sup>4</sup> and Massimiliano Rinaldo Barchi<sup>3</sup>

5 <sup>1</sup>Istituto Nazionale di Geofisica e Vulcanologia, Roma, 00143, Italy

6 <sup>2</sup>GFZ, German Research Centre for Geosciences, Telegrafenberg, 14473, Potsdam, Germany

7 <sup>3</sup>Dipartimento di Fisica e Geologia, Università degli Studi di Perugia, Perugia, 06123, Italy (Member of CRUST - Centro  
8 interUniversitario per l'analisi SismoTettonica tridimensionale con applicazioni territoriali)

9 <sup>4</sup>EarthScope Consortium, Boulder, CO, 80301, USA

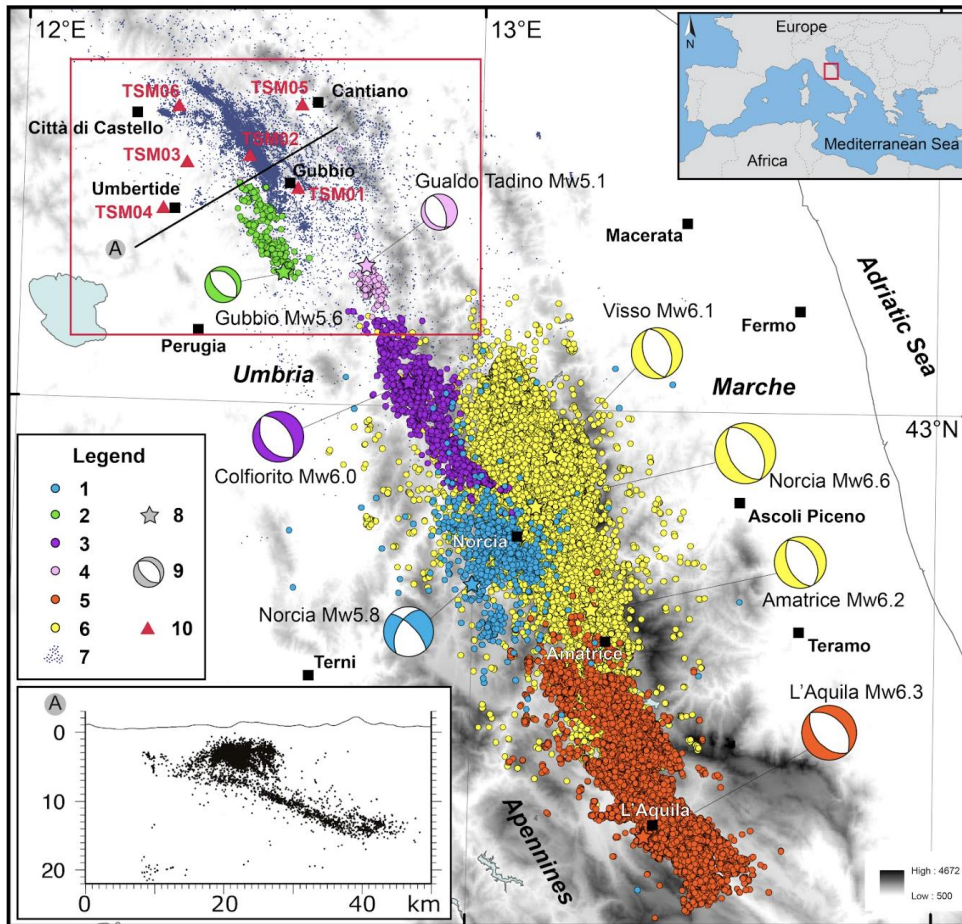
10 *Correspondence to:* Paola Montone ([paola.montone@ingv.it](mailto:paola.montone@ingv.it))

11 **Abstract.** The ICDP STAR drilling project aims to study the seismic and aseismic fault slip behaviour of the active low-angle  
12 Alto Tiberina normal Fault (ATF) in the Northern Apennines, Central Italy, drilling and instrumenting six shallow boreholes  
13 ([maximum depth 160 m](#)) with seismometers and strainmeters. During the STAR field work, a geophysical downhole logging  
14 campaign was carried on defining the optimal target depth for instrument deployment and formation rock characterization. In  
15 particular, the main objectives of this study were to define in situ physical properties of the rocks and the tectonic discontinuity  
16 geometry along the boreholes. The downhole logging data provide new findings and knowledge especially with regards to the  
17 physical properties such as resistivity, gamma ray and wave velocity. The collected parameters were compared to the results  
18 of literature data collected in similar lithologies, as well as with the results of logging performed in deeper wells drilled for  
19 commercial purposes. The physical properties of the Mesozoic-Early Tertiary calcareous formations show low Gamma Ray  
20 values and high compressional ( $V_p$ ) and shear wave ( $V_s$ ) velocities (up to 5.3 km/s and 2.9 km/s, respectively), whereas the  
21 overlying clay-rich Late Tertiary formations exhibit high Gamma Ray and low resistivity and relatively low  $V_p$  and  $V_s$  values  
22 (up to 3.5 km/s and 2.0 km/s, respectively). The results obtained from the analysis of the orientations of the tectonic structures,  
23 measured along the six boreholes, show a good agreement with the orientations of the present-day extensional stress field, NE-  
24 SW oriented. Our study allowed to bridge the gap between the physical properties obtained from literature data and those  
25 obtained from the deep wells measurements, representing a possible case history for future projects. These new [outcomes data](#)  
26 [represent an almost unexplored window of data and](#) will contribute to the advancement of knowledge of the physical properties  
27 of the rocks at shallow depths, typically overlooked. ↓

Formatted: Font: 10 pt, Not Bold

30 **1 Introduction**

31 The aim of the STAR drilling project (A Strainmeter Array Along the Alto Tiberina Fault System) is to study seismic and  
32 aseismic slip on active high- and low angle seismogenic normal faults (Chiaraluce et al., 2024<sup>3</sup>) in Central Italy, an area  
33 affected by seismic events with magnitude up to Mw 6.6 (Fig. 1). The STAR drilling project is an international effort  
34 contributing to the infrastructural implementation of the Alto Tiberina Near Fault Observatory (TABOO-NFO) (Chiaraluce et  
35 al., 2014a, 2014b; Chiaraluce et al., 2022), a long-term research infrastructure mapped by the EPOS ([European Plate Observing  
36 System](#)) initiative as one of the European Solid Earth Science facilities providing open access data to the international  
37 community (<http://www.epos-eu.org>). STAR is one of the International Continental Scientific Drilling Program ([ICDP](#))  
38 projects with a primary focus on long-term borehole monitoring of fault-zone deformation (e.g., Bohnhoff et al., 2017; Fischer  
39 et al., 2022).



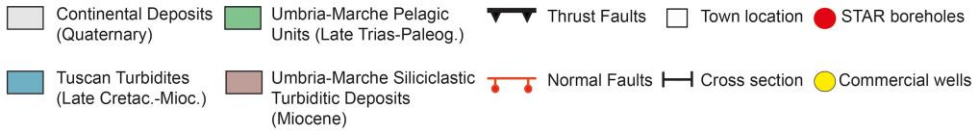
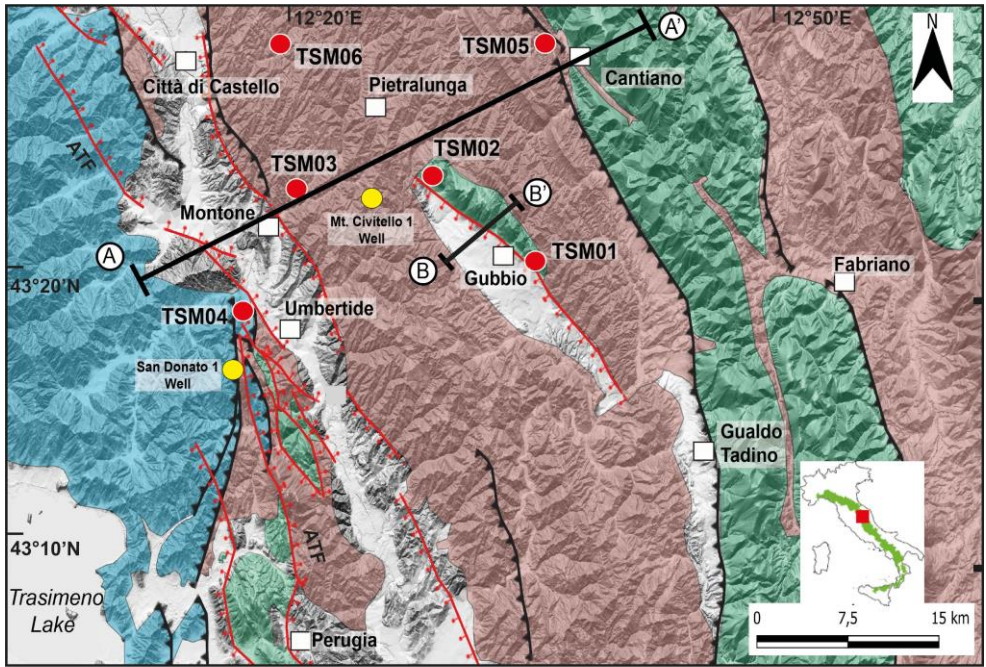
40  
 41 **Figure 1: Seismicity in the study area and main seismic sequences in central Italy in the last 45 years. Legend: From 1**  
 42 **to 6: 1- Norcia 1979 (Deschamps et al., 1984); 2- Gubbio 1984 (Haessler et al., 1988); 3- Colfiorito 1997 (Chiaraluce et**  
 43 **al., 2003); 4- Gualdo Tadino 1998 (Ciaccio et al., 2005); 5- L'Aquila 2009 (Valoroso et al., 2013); 6- Central Italy 2016-**  
 44 **17 (Michele et al., 2020); 7- seismicity in the period 2010-2014 (Valoroso et al., 2017); 8 and 9- location of main events**  
 45 **of the sequences and related focal mechanisms (Italian CMT dataset; Pondrelli and Salimbeni, 2006; Pondrelli et al.,**  
 46 **2006; Quick Regional Moment Tensors); 10- STAR boreholes (TSM). The red box is the area of Figure 2. In the lower**  
 47 **left corner, a cross section of the seismicity (Michele et al., 2020).**

48

49 To improve the comprehension of the processes controlling fault mechanics and earthquake generation, the STAR drilling  
50 project installed short period (2Hz) seismometers (three-component borehole geophones) and strainmeters (Gladwin Tensor  
51 Strainmeters, GTSM) in six shallow boreholes (maximum depth 160 m) purpose-drilled. The seismometers were installed to  
52 monitor and record [the](#) seismicity of the low-angle Alto Tiberina normal Fault (ATF) and its main antithetic splay, the Gubbio  
53 normal fault (Mirabella et al., 2004; Caricchi et al., 2015) (Fig. 2). Borehole strainmeters were deployed because they are the  
54 only instruments able to measure small creep events, as demonstrated in similar experiments focused on other faults, such as  
55 the creeping section of the strike-slip San Andreas fault near Parkfield (Langbein et al., 2006). [The small creep events can be  
56 recorded by strainmeters whose high resolution, for periods of hours to ~10 days, enables the identification of subtle, time-  
57 varying crustal deformations that are too small to be measured by GNSS or InSAR.](#)

58 Seismic and strain observations from the STAR boreholes monitoring will be integrated with regional observations on active  
59 seismicity, on deep crustal structure and on the present-day stress field.

60 The locations of the six boreholes were selected based on two main criteria: on a regional scale, the objective was to enhance  
61 understanding of the seismic behaviour of the ATF; on a local scale, the primary requirement was to deploy the instruments  
62 while avoiding areas of inhomogeneous, anisotropic, or highly fractured rock volumes (Chiaraluca et al., 2024). The six 80-  
63 160 m shallow monitoring boreholes, named TSM01-06, (see locations in Figure 1) were drilled surrounding the creeping  
64 portion of the ATF in two phases: during the Fall of 2021 and Spring of 2022. The STAR drilling operations were supported  
65 by the acquisition in all the boreholes of a wide set of geophysical logs including: optical (OBI), acoustic (ABI), caliper (CAL),  
66 gamma ray (GR), fluid temperature conductivity (FTC), sonic (FWS), resistivity and spontaneous potential (ELOG) logs. The  
67 borehole geophysical measurement purposes for the STAR drilling project were twofold: firstly, to characterise the physical  
68 properties of the rock formation in the subsurface and, secondly, to identify an intact and competent fracture-free interval in  
69 each borehole in which to deploy the strainmeter and seismometer. After the completion, each borehole was instrumented and  
70 ready for data acquisition (Chiaraluca et al., 2024).



71  
 72 **Figure 2: Geological setting of the study area. The location of the six STAR boreholes (red circles) drilled in Fall 2021 (TSM01, 02,**  
 73 **and 03) and in Summer 2022 (TSM04, 05, and 06), and two deep commercial boreholes (yellow circles), San Donato 1 and Mt.**  
 74 **Civitello 1, are displayed. Modified from (Mirabella et al., 2011). ATF is the Alto Tiberina fault. The geological cross-sections A-A'**  
 75 **and B-B' are in Fig. 3.**

76  
 77 The objective of this paper is to provide a critical overview of the physical properties of the in-situ rock formations and their  
 78 fracture characteristics based on analysis and interpretation of downhole logging data. Particular attention was paid to optical  
 79 and acoustic image logs with the aim of identifying intact rock and structural discontinuities. In fractured rock masses,  
 80 discontinuities have significant control over the rock mass behaviour. Mapping at depth the fractures and their geometry helped  
 81 us identify optimal intervals to host seismometers and strainmeters. In order to work properly and obtain reliable data, these

82 instruments must have a perfect coupling with the rock mass: therefore, borehole seismic installations have to take into account  
83 the borehole diameter and tilt, temperature profile, lithology and fracture distribution.

84 In this paper, after a brief description of the seismicity of central Italy and a geological and tectonic overview of the area where  
85 the boreholes are located, we describe the main results of the operated logging. Geophysical downhole measurements provide  
86 a contribution to better define the physical properties of the Umbria-Marche carbonate multilayer (mainly limestones and  
87 marls) and of the overlying turbidites, cropping out in this area. These results are then compared with the analogue  
88 measurements, acquired in much deeper boreholes, drilled in the same region for hydrocarbon exploration purposes, as well  
89 as with the available, recently acquired laboratory measurements (e.g. De Paola et al., 2009; Smeraglia et al., 2014; Trippetta  
90 et al., 2010, 2021) ~~that give insights into giving food for thought about~~ the effects of the confining pressure on the physical  
91 parameters of the rocks. In particular, the results related to the P-wave velocities obtained from the sonic log readings along  
92 the six STAR boreholes have been compared with the previous results related to the same geological formations (e.g. Barchi  
93 et al., 1998; Diaferia et al., 2006; Bigi et al., 2011; Mirabella et al., 2011; Scisciani et al., 2014; Porreca et al., 2018; Montone  
94 and Mariucci, 2020; Trippetta et al., 2021). From the geophysical log analysis, we have defined and characterised several  
95 planar discontinuities along each borehole, related either to primary (bedding) or to secondary (tectonic) structures (fault and/or  
96 fractures). The orientations of the tectonic structures, recognized along the boreholes, have been considered together with other  
97 available data and compared with the present-day stress field.

98 Summarising, our paper aims to bridge the gap between the physical properties obtained from literature data (e.g. laboratory  
99 analyses) on outcrop samples and those obtained from the wellbore measurements of oil and gas companies (such as AGIP,  
100 ENI; <https://www.videpi.com/videpi/pozzi/consultabili.asp>), which investigate significantly greater depths. The new data of  
101 this study will contribute to the advancement of knowledge of the physical properties of the rock ~~volumemasses~~ at relatively  
102 shallow depths (0-200 m), typically overlooked. ~~Beyond the specific case reported here, geophysical and petrophysical data~~  
103 ~~acquired in shallow boreholes also contribute to the knowledge of the upper crust. Indeed, they provide in situ measurements~~  
104 ~~linking those obtained on outcropping rocks, often influenced by surface processes, with those from deep wells. Our study~~  
105 ~~shows how even with relatively few data in a large area, valuable insights can be obtained. With more data in a region of~~  
106 ~~interest, we would be able to shed a light on a complete portion of the crust, from surface to few kilometres depth, or even~~  
107 ~~deeper.~~ Overall, also considering the results obtained in the analysis and interpretation of the data in this study, the outcomes  
108 from the STAR drilling project will provide a better understanding of the behaviour of the main active faults, addressing  
109 fundamental questions about the relationship between creep, slow slip, dynamic earthquake rupture, and tectonic faulting  
110 ([Anderlini et al., 2016](#); [Chiaraluca et al., 2023](#)).

Formatted: Font color: Auto

## 2 Seismotectonic and geological framework of the area

Seismicity in Central Italy is mainly characterised by shallow crustal earthquakes (5–15 km depth) localised along the Apennine belt with maximum magnitudes of about 6.6 (Chiarabba et al., 2005; Chiaraluze et al., 2017a). Earthquake focal mechanisms show a prevalent normal faulting regime, with a NE–SW striking extension, consistent with other data characterising the active stress field in this area, such as breakouts and active faults (Mariucci and Montone, 2024).

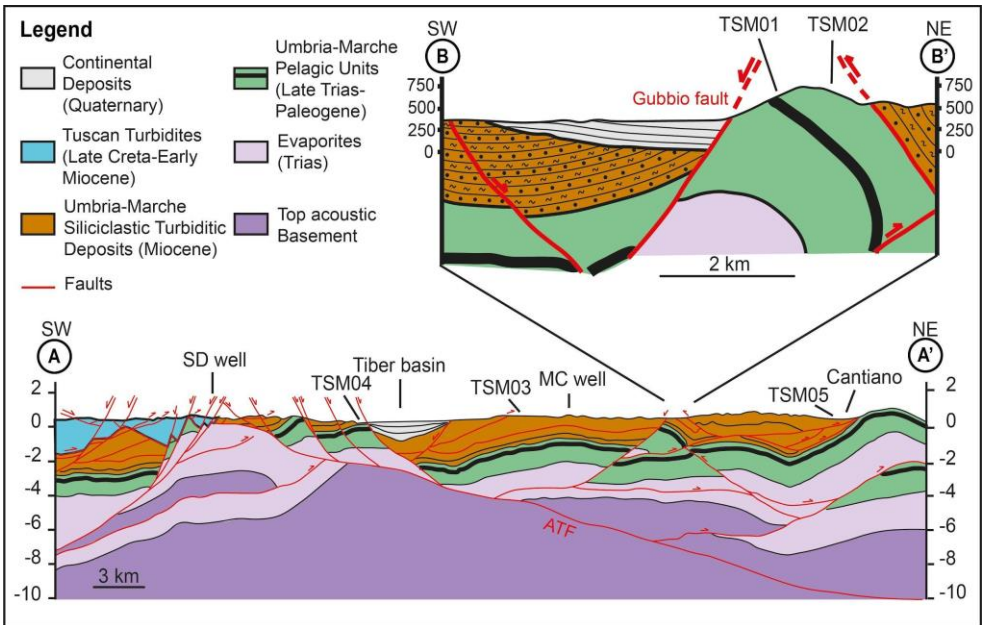
In the last 45 years, Central Italy has experienced several crustal normal-faulting earthquakes (Fig. 1) causing surface faulting as well, visible fractures and significant damage (Cinti et al., 1999; Barchi and Mirabella, 2009; Boncio et al., 2010; Emergeo working Group, 2010; Pizzi et al., 2017; Villani et al., 2018; Barchi and Collettini, 2019). The most significant earthquakes occurred in the past, with a moment magnitude greater than 5.5 (Fig. 1), are the Mw 5.8 Norcia in 1979, the Mw 5.6 Gubbio in 1984 and the seismic sequence of Colfiorito-Gualdo Tadino in 1997-98, with the largest event Mw 6.0 (Cello et al., 1997; Amato et al., 1998; Amato and Cocco, 2000; Boncio and Lavecchia, 2000; Ciaccio et al., 2005; Mildon et al., 2016). Finally, the seismic sequence that began in 2016 in Amatrice (Tinti et al., 2016; Chiaraluze et al., 2017b; Chiarabba et al., 2018) occurred with three main events (Mw 6.2 in Amatrice, Mw 6.1 in Visso, and Mw 6.6 in Norcia), causing about 300 deaths, injuries and the destruction of numerous historic centres (Fig. 1).

The six boreholes of the STAR drilling project were drilled in the NW part of the actively extending area of the Umbria-Marche Apennines (Fig. 2), a NE-verging, arc-shaped foreland fold-and-thrust belt, representing the eastern part of the Northern Apennines of Italy. Within the study area the compressional structures (folds and thrusts) are mostly arc-shaped with a roughly NNW-SSE trend and were formed in Late Miocene (Tortonian-Messinian age). They affect a pre-orogenic Jurassic-Paleogene carbonate multilayer (Umbria-Marche succession) (e.g. Cresta et al., 1989), overlain by a thick succession of syn-orogenic Neogene turbidites, marls and sandstones, deposited in the Northern Apennines foreland basin (e.g. Barchi, 2010). The compressional structures are cut and displaced by later (Late Pliocene-Quaternary) NW-SE striking normal faults, which are related to an extensional stress field oriented in a NE-direction, responsible for the present-day seismicity of the region. The normal faults attitude is consistent with the extensional stress regime inferred from earthquake focal mechanisms and borehole breakouts (Mariucci et al., 2008; Montone and Mariucci, 2016; Villani et al., 2018).

The most prominent normal fault exposed in the study area is the SW-dipping Gubbio fault, down-throwing the western backlimb of the Gubbio anticline (Fig. 3). The Gubbio fault is antithetic to a major NE-dipping extensional detachment, i.e., the ATF (e.g. Mirabella et al., 2011; Lavecchia et al., 2017; [Vuan et al., 2020](#)). The fault dip of less than 30° makes the ATF an unfavourably oriented geological structure for reactivation with respect to the regional stress field. The ATF and its high-angle antithetic splays release continuous microseismicity, and rarer moderate sequences, e.g. in 1984 (Haessler et al., 1988) and in 2010-2014 (Marzorati et al., 2014).

The stratigraphy of the study area, from top to bottom, can be summarised as follows (Barchi, 2010): i) marine and continental Plio-Quaternary sediments, mainly clays and sands in different combinations and with different degrees of compaction; ii) a thick Neogene synorogenic turbidite succession, namely Marnoso-Arenacea Fm. (Miocene), formed of alternated shales and

146 sandstones, with strong vertical and lateral variability; iii) a hemipelagic marly succession (Schlier, Bisciario and Scaglia  
 147 Cinerea Fms.; Eocene -Miocene); iv) a carbonate pelagic sedimentary sequence of the Umbria–Marche domain (Mesozoic–  
 148 Paleogene) that includes not only limestone and chert-bearing limestone but also marl and clay (Scaglia Variegata, Scaglia  
 149 Rossa, Scaglia Bianca, Marne a Fucoidi and Maiolica Fms.); v) Lower Jurassic massive platform carbonate (Calcare Massiccio  
 150 Fm.); vi) Upper Triassic evaporitic succession, consisting of alternated anhydrites and dolostones (Anidriti di Burano Fm.);  
 151 vii) Middle Triassic and/or older continental and shallow marine meta-sediments (Verrucano Fm. s.l.).



152  
 153 **Figure 3: Geological cross-sections (A-A' and B-B' in Figure 2). The geometry at depth of the main tectonic structures such as the**  
 154 **Alto Tiberina low angle normal fault (ATF) and the Gubbio fault (Mirabella et al., 2011) are shown. SD well, San Donato 1 well;**  
 155 **MC well, Mt. Civitello 1 well.**

156  
 157 Within the STAR study area (Figures 2 and 3), two deep wells (San Donato 1 and Mt. Civitello 1) were drilled in the past by  
 158 Italian oil Companies. The wells stratigraphy is schematically reported in previous literature (e.g. Mariucci et al., 2008;  
 159 Mirabella et al., 2011; Caricchi et al., 2015). The San Donato 1 well (SD), reaching a depth of 4763 m, was drilled by SNIA-  
 160 BPD in 1983-84 and is located approximately 20 km southwest of the Mt. Civitello 1 well (MC). The SD well is situated very  
 161 close to the ATF, intersecting it at a depth of 326 m, where the Miocene Marnoso-Arenacea turbidites directly overlie the



162 Triassic evaporitic succession, extending down to a depth of about 3000 m. At greater depth, the well penetrates the  
163 metamorphic acoustic basement in tectonic contact with the evaporitic succession (Fig. 3). The MC well, drilled by AGIP in  
164 1988-89, located near the Gubbio fault, reaches a depth of 5600 m. From the surface to a depth of about 1000 m, the well  
165 crosses the turbidite succession. Then the well passes through the carbonate Meso-Cenozoic pelagic sequence. From about  
166 2800 m to the bottom at 5600 m, the well crosses the Triassic evaporitic succession.  
167

### 168 **3 Method: downhole logging processing and analysis**

169 The knowledge of the petrophysical properties of the different litho-stratigraphic units is an important aspect to understand  
170 the subsurface. In the lack of coring material, as in the STAR project, data acquisition from downhole logging becomes the  
171 key element in determining the rocks physical characterization (i.e. Rider and Kennedy, 2011). Downhole logging is a method  
172 to gain continuous, in situ high-resolution data of various physical or structural rock parameters collected within a borehole.  
173 For the STAR drilling project, the downhole logging was performed for all six boreholes in order to allow detailed sedimentary  
174 facies assessment and to identify the best location to deploy the strainmeters and seismometers at depth. All six boreholes were  
175 logged by slimhole sondes (for details see Table S1 and text in the Supplementary), and following the standard methods in this  
176 field (Serra, 1984; Ellis and Singer, 2007; Rider and Kennedy, 2011; Schön, 2015; Pierdominici and Kück, 2021). Downhole  
177 measurements were conducted in each borehole after the drilling operations and executed mainly in the open hole (OH)  
178 sections, only GR ran also in the cased section (CH). The following downhole measurements were successfully recorded: total  
179 gamma ray (GR), full waveform sonic (Vp and Vs), temperature (T) and ~~conductivity~~ ~~conductibility~~-(COND), three-arm  
180 caliper (CAL), resistivity (RESIST), single point resistance (SPR), and acoustic (ABI) and optical images (OBI). We have  
181 summarised the logging measurements and logged interval for each borehole in Table S1. For the drilling operations, water  
182 was used as drilling fluid allowing to run the OBI. Borehole quality has been determined by vertical and horizontal deviation  
183 of the borehole and the condition of the borehole wall. In order to pursue the objective of the STAR drilling project and for  
184 proper use and performance of the instruments, all six boreholes were drilled within 5° from the vertical. The deviation of each  
185 borehole was then checked as part of the logging program. The boreholes have an inclination of less than 2° except for the  
186 borehole TSM06 where the inclination is between 4.3° and 5.1°. Based on i) the smooth borehole wall, ii) log without intervals  
187 of large washouts and iii) internal consistency for several tools (i.e., three different types of borehole diameter measurement),  
188 we infer that the log quality and reliability are very good for almost all sondes over the entire length of each hole.

189 Below, we have summarised the main scientific purpose of each sonde.

190 The total gamma ray log (GR) measures the natural radioactivity of the rock. The GR comes from the radioactive isotopes of  
191 potassium (40K), uranium (238U decay series) and thorium (232Th decay series). Potassium is found primarily in clay  
192 minerals, micas, and potassium feldspar; thorium is commonly associated with clay minerals and volcanic ash layers; uranium

193 is found in heavy minerals, glauconite and organic rich intervals and may be bound to clay. Relatively high values in GR log  
194 are often associated with the influx of clay and coarser materials, while relatively low GR values generally indicate  
195 sedimentation of biogenic carbonate, organic carbon, or silica (e.g. Rider and Kennedy, 2011). We performed the GR log to  
196 detect layers of clay and to identify changes in lithology. GR was also recorded in drill pipes of all six STAR boreholes,  
197 although the signal appears a bit dampened. In essence, GR log characterises the different lithology crossed by the borehole  
198 allowing to identify layers (thickness and lithotype) through the different clay content.

199 A three-arm caliper (CAL) sonde was used to measure the borehole diameter and to determine how smooth the borehole walls  
200 are. The strainmeter requires relatively smooth walls with no blowouts or fractures.

201 The fluid temperature-conductivity (FTS) measures the temporary temperature and conductivity of the borehole fluid. Both  
202 parameters can show strong variations caused by drilling activities inside the hole but also can detect flow of fluids into or out  
203 of the formation. These logs are good indicators of areas of active flow or open fractures, therefore are used to exclude areas  
204 or intervals with major fractures that would have affected both instrument placement and data quality.

205 The ELOG sonde - including RES and SPR - measures the rock capability to conduct electric currents. The tool provides  
206 resistivity profiles with four different depths of investigation. This measurement provides information about permeability,  
207 porosity, water types and geological formation properties. In particular, in massive rocks with very low matrix  
208 porosity/permeability, the resistivity logs identify fluid filled fracture zones (fracture permeability). So, we ran this logging  
209 sonde for the same reason as the FTS. Only for the TSM01 and TSM02 boreholes the ELOG logs were not acquired.

210 The Full Waveform Sonic (FWS) sonde measures the velocity of sound waves through the rocks, which varies depending on  
211 lithology, rock texture and porosity. The sonic velocity measurement is used for identification of compaction of lithologies,  
212 facies recognition and fracture identification. The velocity has been determined by measuring the travel time of sonic pulses  
213 between transmitters and four receivers. We have reprocessed the raw sonic waveforms to estimate the P and S-wave velocities  
214 using a combination of first arrival trace picking for P and S waves, along with additional semblance analysis.

215 Borehole image sondes provide a continuous oriented high resolution image of the borehole walls ([see the figures related to](#)  
216 [the boreholes, e.g., Fig. 6](#)). Images collected in the STAR project have been obtained from acoustic (ABI) and optical (OBI)  
217 tools. The latter acquires a true-colour optical image of the borehole wall, and the acquired data are displayed in one oriented  
218 unwrapped image. The sonde operates only in a transparent drilling fluid like fresh water or air. For TSM04 and TSM06  
219 boreholes no optical image is available due to the high turbidity of the drilling water. The acoustic image data are visualised  
220 as two 360 degrees north-oriented images (travel time and amplitude) of the borehole wall versus depth. The travel time (TT)  
221 provides information about the borehole shape and the acoustic amplitude (AMPL) depends on the roughness and shape of the  
222 borehole wall and its acoustic properties, which depend on variations with texture, mineralogy, compaction, and fracturing  
223 (e.g. Davatzes and Hickman, 2010; [Mcginnis et al., 2017](#); [Medici et al., 2023](#)). These AMPL and TT images are visualised in  
224 colours based on their value range. Here, in the AMPL image, strong contrast (high amplitude, bright colour) indicates a strong  
225 signal and good reflection, and low contrast (low amplitude, dark colour) indicates weak to missing signals (scattered or

226 absorbed impulse). In the TT image, the bright colours indicate a short time period (fast) for the impulse to go from the  
227 transducer and back to the receiver; the dark colours represent a long time period (slow), which means widened size of the  
228 borehole (e.g. Pierdominici et al., 2020). Each planar discontinuity, such as fracture, fault, bedding, appears in the images as  
229 sine waves (e.g. Davatzes and Hickman, 2010). To obtain a correct geometry of the planar structures (dip azimuth and dip) the  
230 TT and AMPL images have been prior corrected by diameter, inclination and orientation of the borehole. We have grouped  
231 the features in six categories (see Section 4.3): open (in red), filled (in grey), bedding (in green), stylolite (in turquoise), cherty  
232 layer (in dark grey) and weak zones. The acoustic imager tool alone cannot distinguish between open or closed/filled structures  
233 (used here in a general term, i.e., including faults, fractures, and veins). Based on the comparison of these two images, we  
234 might distinguish so-called “open” structures based on their contrast of ultrasonic AMPL and the corresponding response in  
235 the TT. The structures defined as “closed” are visible only in the amplitude image. To enhance the travel time and amplitude  
236 images, static and dynamic (10 cm vertical window) normalizations were applied. Raw, static, dynamic images display minor  
237 differences of each other in the resulting images depending on the scale and variations between different intervals and features.  
238 The displayed images here refer to the static normalisation. The ABI and OBI were also used to determine the borehole  
239 trajectory based on borehole's deviation from vertical (DEVI) and the direction of this deviation with respect to magnetic north  
240 (hole- or drift-azimuth; HAZI). For the installation of strainmeters and seismometers, all STAR boreholes had to be very close  
241 to the vertical. Thus, this type of acquisition played a key role in knowing the condition of the borehole and decreeing the  
242 successful installation of the instruments.

## 243 4 Data and Results

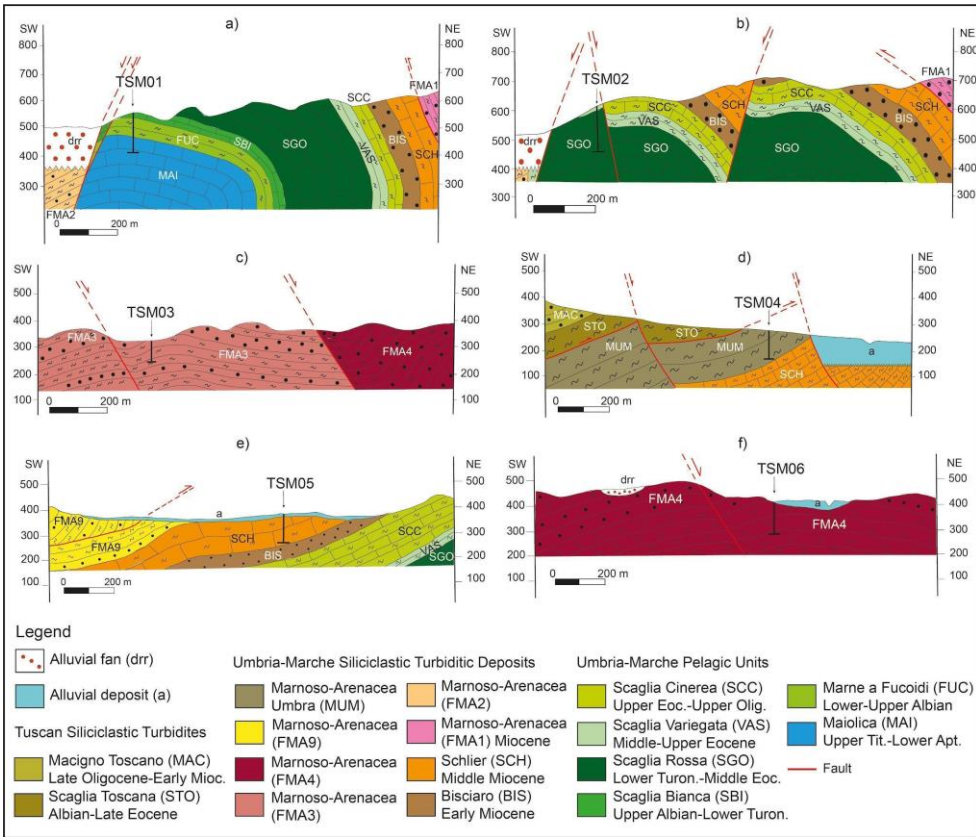
### 244 4.1 Borehole description

245 Six STAR boreholes were drilled surrounding the creeping portion of the ATF to deploy strainmeters and seismometers (Fig.  
246 1) in order to improve our understanding of the ATF seismicity pattern and monitor the evolution of seismicity in this area  
247 over time (Chiaraluca et al., 2024). For the location of our six boreholes we have followed two criteria: at a regional scale,  
248 three boreholes (TSM01, 02 and 06) are located following the axis of the Gubbio anticline and its northern continuation and  
249 the others (TSM03, 04 and 05) where the maximum extension rate is expected. At a local scale, the instruments were deployed  
250 in relatively homogeneous lithology, avoiding complex formations (e.g. alternating stiff and weak rocks or limestones and  
251 marl layers) as well as anisotropic or highly fractured rock intervals. The downhole logging measurements were performed  
252 immediately after drilling and prior to instrument installation. A posteriori, the known mechanical properties of the rocks  
253 hosting the instruments will be used to improve the interpretation of the data recorded.

254 The boreholes are located within an area of about 1500 km<sup>2</sup>, centred around the town of Gubbio (Fig. 2 and Table S2). Among  
255 the six new boreholes, TSM01 and TSM02, near the Gubbio fault, were drilled across the late Mesozoic-Early Tertiary  
256 carbonates, cropping out along the crest of the Gubbio anticline, which represents the maximum structural culmination of the

Formatted: Font color: Custom Color(RGB(56,118,29)),  
Highlight

257 study area (Fig. 4 a, b). The other boreholes were drilled in the Tertiary marls and sandstones, cropping out in the northern  
 258 part of the study area: TSM04 is located on the footwall of the ATF, TSM03 and TSM06 were drilled on the ATF hangwall,  
 259 and TSM05 is located in the farthest part of the ATF, close to the western flank of the Umbria-Marche ridge (Fig. 4 c, d, e and  
 260 f.; for more detail, see Chiaraluca et al., 2024).  
 261 See supplementary files for a lithological detailed description (Supplementary 1).



262  
 263 **Figure 4: Geological cross-sections across the STAR boreholes. Different members of Marnoso-Arenacea Fm. are shown (FMA1, 2,**  
 264 **3, 4, 9 and MUM).**

265

266 **4.2 Log results**

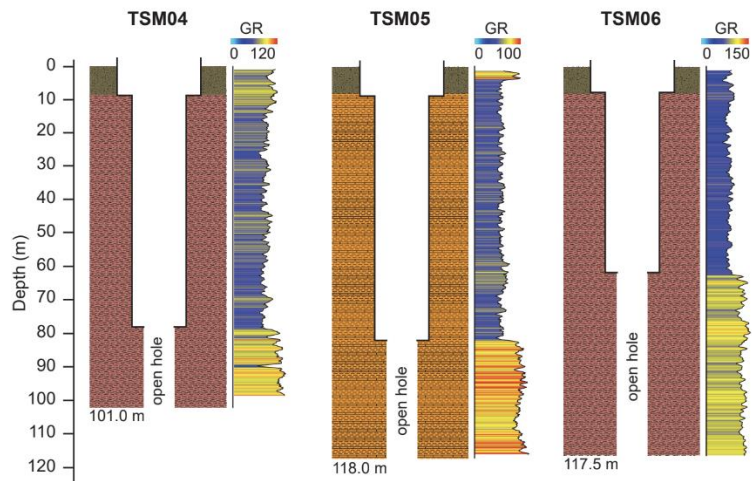
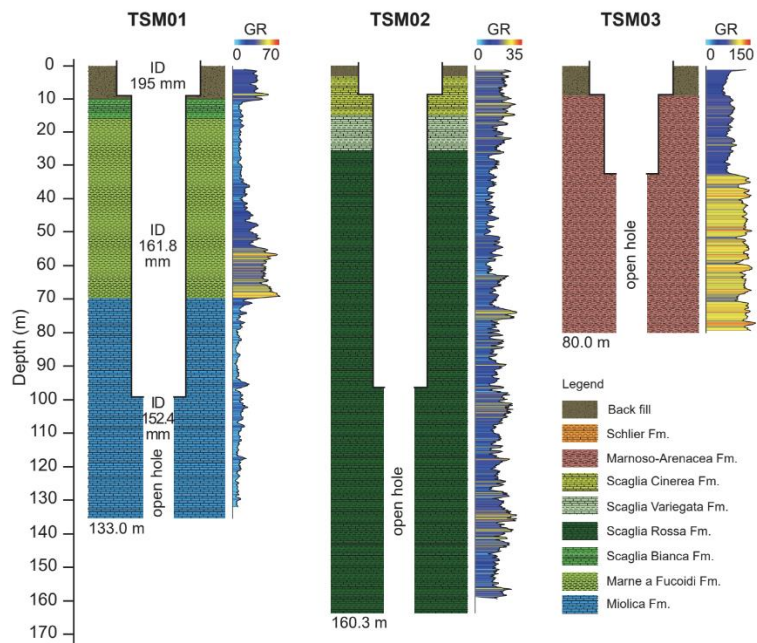
267 The downhole logging data are described and interpreted to provide new findings and knowledge to complement those obtained  
 268 from similar rock types sampled in the field outcrops (Fig. 5 and Figs. 6-9).

269 Results from the downhole logging analysis are summarised in Table 1 and Table S1 displaying the average values and the  
 270 related standard deviation. More details are described in Supplementary 2.

Boreholes	ICDP-ID	Lithological Formation*	Depth m		GR cps		Vp m/s	Vs m/s	RES Ωm	SPR Ωm	T °C	COND μS/cm
			CH	OH	CH	OH						
TSM01	5070_1_A	Maiolica	0.0-99.3	99.3-133.0	17.9±13.3	8.4±4.4	5324±371	2885±112	n.d.	n.d.	12±1	381±40
TSM02	5070_2_A	Scaglia Rossa	0.0-97.0	97.0-160.3	11.7±5.4	13.4±5.6	4867±184	2505±500	n.d.	n.d.	15±1	456±62
TSM03	5070_3_B	Marnoso-Arenacea	0.0-32.0	32.0-80.0	61.5±12.7	104.2±15.9	3204±168	1800±130	29±5	104±10	14±0.2	452±7
TSM04	5070_4_A	Marnoso-Arenacea	0.0-79.3	79.3-101.0	61.5±10.0	85.1±13.2	2972±207	1993±118	9±1	42±5	16±0.3	694±92
TSM05	5070_5_A	Schlier	0.0-82.3	82.3-118.0	48.6±8.7	81.2±9.3	3451±160	1879±148	12±3	53±7	17±1	634±8
TSM06	5070_6_A	Marnoso-Arenacea	0.0-80.0	80.0-117.5	62.4±9.2	99.7±9.35	3422±306	1896±119	18±3	76±9	18±0.03	487±34

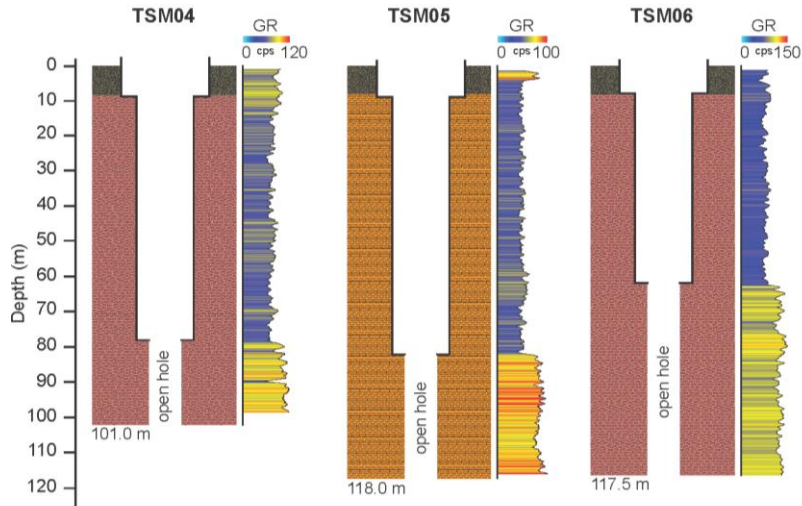
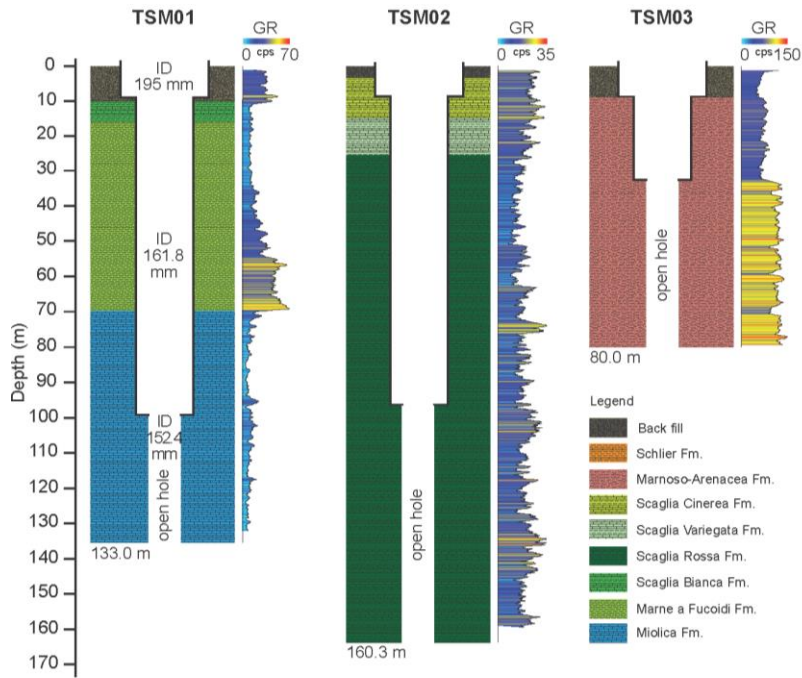
271 **Table 1: Geophysical properties of the rocks for TSM boreholes. GR: gamma ray (count per second); Vp and Vs: P- and S wave**  
 272 **velocity, respectively; RES: resistivity; SPR: single point resistance; T: temperature; COND: conductivity; CH: cased hole; OH:**  
 273 **open hole. \*The lithological formations refer to the open hole section. n.d stands for no data**  
 274  
 275

276 GR log response (open and cased hole) in TSM01 and TSM02 boreholes is generally very low (Fig. 5, Table 1). In TSM01,  
 277 the low GR, associated with the limestone Scaglia Bianca Fm., slowly increases in the marly Marne a Fucoidi Fm.,  
 278 proportionally to the enrichment of the clay component as well evidenced in the interval between 55.0 m and 66.5 m. The  
 279 sharp contact between the Marne a Fucoidi Fm. and the underlying limestone Maiolica Fm. is well indicated by the dramatic  
 280 decrease in GR values (from 50 cps of Marne a Fucoidi Fm. to 14 cps of Maiolica Fm.). The open-hole section interests only  
 281 the Maiolica Fm. with an average GR value of 8.4 cps. In TSM02, GR records a very low response related to the three pelagic  
 282 formations intersected, predominantly consisting of limestones, which are interbedded with sporadic, relatively thin marly  
 283 layers as recorded by the increase in GR values (e.g. 73-75 m, 102-104 m, 134-135 m in Scaglia Rossa Fm.). In the TSM03,  
 284 TSM04, TSM05 and TSM06 boreholes, GR log shows higher values which vary between 49 cps in TSM05, and 104 cps (open  
 285 hole) in TSM03. The GR values are lower in the cased section because the signal is damped by casing. In the open-hole section,  
 286 on the other hand, the GR response for all the four boreholes is generally high, displaying relatively uniform cps value ranging  
 287 between 81 and 104. Intervals with low GR are few and restricted and likely associated with the presence of fractures and/or  
 288 thin sandstone layers. The highest GR values are almost exclusively associated with the marly layers that dominate the  
 289 Marnoso-Arenacea Fm. (TSM03, TSM04 and TSM06) and the Schlier Fm. (TSM05).



291 Figure 5: STAR boreholes with lithostratigraphic profile and gamma-ray log. Each borehole has a conductor casing for the first 9  
292 m, followed by a casing and an open-hole section. ID: inner diameters. Only the total gamma (GR, here shown: [unit: cps - counts](#)  
293 [per second](#)) was also run through the casing, while all other measurements were performed only in the open hole. Seismometers and  
294 strainmeters were deployed at the bottom of the open section of each borehole (for details see Fig. S1).

p95



Formatted: Font: 10 pt, Not Bold, Font color: Auto



297 P (Vp) and S (Vs) wave velocities obtained from the full wave sonic log were measured in the open-hole section down to the  
298 bottom of the hole showing a wide range of values between different boreholes: Vp varies between 2972 and 5324 m/s and Vs  
299 between 1800 and 2884 m/s (Table 1; Figs. 6-9). Higher values were recorded along the boreholes that intersected more  
300 competent lithologies, especially limestones as Maiolica Fm. in TSM01 and Scaglia Rossa in TSM02. A significant decrease  
301 of both Vp and Vs was detected at open fractures occurrence. The dynamic Poisson ratio was computed using the specific  
302 formula from shear and compressional [wave velocities from](#) sonic logs to compare it to the fracture porosity. As expected,  
303 rocks with a low Poisson's ratio show a higher fracture density (Figs. 6-9).

304 Resistivity was measured in TSM03, TSM04, TSM05 and TSM06 boreholes. The values vary from 9 to 29  $\Omega\text{m}$  according to  
305 the response of sonic logs and fracture presence (Table 1); however, with the same lithology the resistivity values vary  
306 following the variations of single point resistance (SPR).

307 Temperature measured in the boreholes (Table 1) is quite constant within a range of 12 to 18°C reflecting the borehole fluid  
308 rather than the “formation temperature”. Due to the shallow investigated depth, the results are not very significant. See Section  
309 3 for details.

310 Conductivity of the drilling fluid is directly proportional to the concentration of dissolved minerals and thus to its salinity: the  
311 highest values (694  $\mu\text{S}/\text{cm}$ ) were found in the TSM04 borehole near the area with intense CO2 emissions of deep origin (Table  
312 1).

#### 313 4.3 Structure analysis

314 In this section we present the analysis of optical and acoustic images performed to identify the main discontinuities along the  
315 boreholes (Figs. 6-9). As mentioned before, we have grouped the features in six categories: open (in red), filled (in grey),  
316 bedding (in green), stylolite (in turquoise), chert layer (in dark grey) and weak zones. The filled and open fractures usually  
317 have a thickness from a few mm up to 1-2 cm. Furthermore, we plotted the main tectonic structures (open and filled fractures  
318 and weak zones) as rose diagrams splitting the data according to their dipping ( $>$  and  $<$  45°).

319 **TSM01.** The analysis of OBI and ABI images allowed us to identify and detect the main discontinuities crossed by the borehole  
320 (Fig. 6). The sub-horizontal discontinuities correspond to bedding planes, while the filled discontinuities can be interpreted as  
321 later-filled fractures or cleavage planes. Moreover, numerous stylolites and chert layers are present within the Maiolica Fm.,  
322 both parallel to bedding. A detail of the main features is shown in the inset of Fig. 6-i. A total of 69 discontinuities (only open  
323 and filled fractures) were recorded along the open-hole section showing a homogeneous distribution along the borehole with  
324 a maximum of 8 structures per metre. The preferential orientation is NW-SE, corresponding to a dip azimuth of N200° (Fig.  
325 10). The dip of these planes is generally low (around 25°), contributing to the azimuthal dispersion of the data. However, some  
326 discontinuities with steeper dips (ranging from 60° to 80°) are still NW-SE oriented.

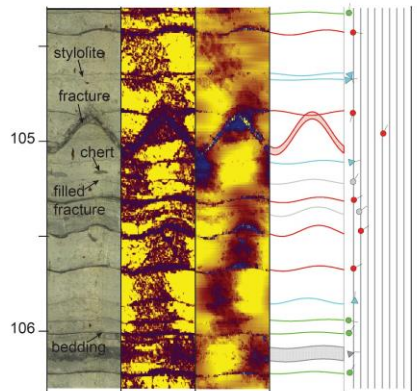
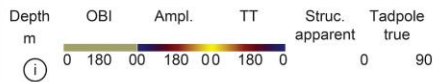
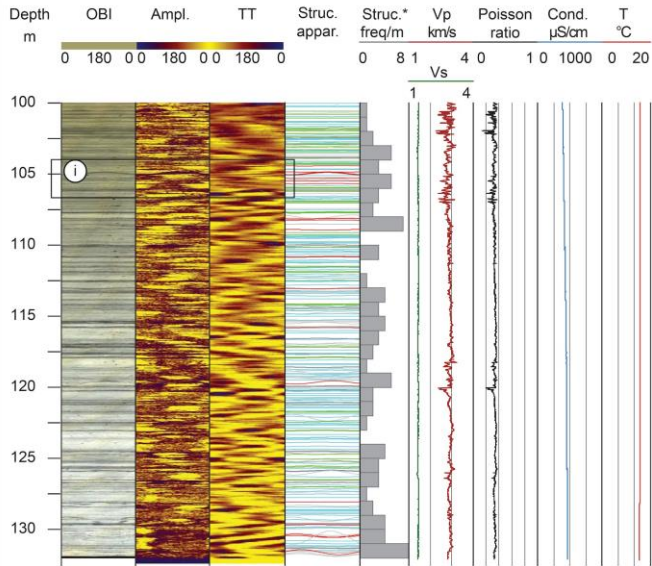
327

Formatted: Font: Not Bold, Font color: Auto

Formatted: Font: Not Bold, Font color: Auto

Formatted: Font: Not Bold

**TSM01**



**Legend**

- OBI optical borehole image
  - Ampl. amplitude
  - TT travel time (from Acoustic Borehole Image)
  - Struc. structures
  - Struc.\* structures frequency
  - Vp, Vs P and S-wave velocity (from the Full Wave Sonic log)
  - Cond. electrical conductivity
  - T temperature
- Structures**
- open
  - filled
  - ▼ styloite
  - ▼ chert layer
  - bedding

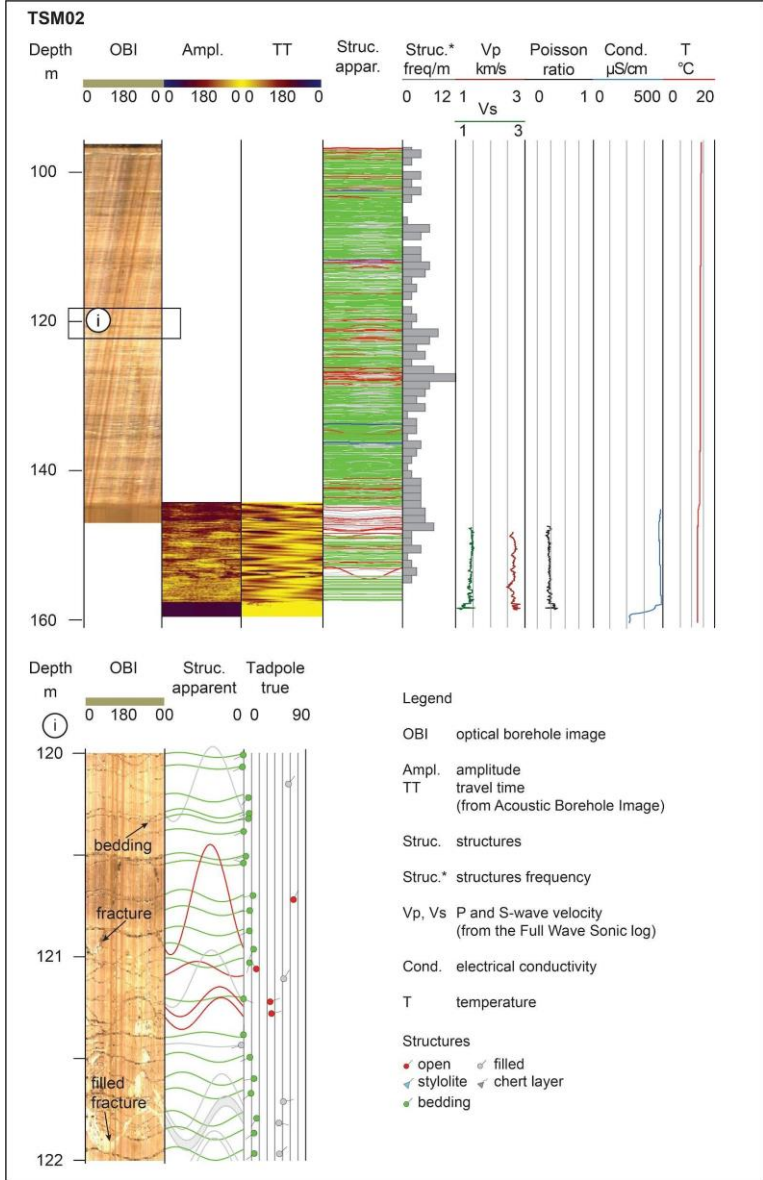
Formatted: Font: 10 pt, Not Bold

Formatted: Font: 10 pt, Not Bold

329 Figure 6. Downhole logging measurements performed along the TSM01 borehole (Maiolica Fm.). At the bottom: a detail of  
330 the structures intersected by the borehole.

331  
332 TSM02. The OBI and ABI images available for structural analysis investigated two different depth ranges. The OBI was  
333 performed from 96.2 to 147.0 m and the ABI from 144.2 to 159.6 m. The OBI image clearly shows continuous and parallel  
334 layering and especially the interlayering of thin clay layers in the limestone. The Scaglia Rossa Fm. is also affected by  
335 numerous thick filled and open fractures. The analysis of the planar discontinuities identified on both images allowed us to  
336 distinguish bedding planes, filled and open fractures (Fig. 7). The latter two structures (195 counts) revealed a predominant  
337 orientation of NNW-SSE, corresponding to a dip azimuth of N204° (Fig. 10), with an average structure frequency of 6 per  
338 metre and a high discontinuities concentration around 120 to 125 m (Fig. 7-i). The majority of open and filled fractures have  
339 dipping values higher than 45°, the open ones dipping almost exclusively to NE, and the closed ones to SW (Fig. 10).  
340

- Formatted: Font: 10 pt, Not Bold, Font color: Auto
- Formatted: Font: 10 pt, Not Bold
- Formatted: Font: 10 pt, Not Bold, Font color: Auto
- Formatted: Font: 10 pt, Not Bold
- Formatted: Font: 10 pt, Not Bold, Font color: Auto
- Formatted: Font: 10 pt, Not Bold
- Formatted: Font: 10 pt, Not Bold, Font color: Auto
- Formatted: Font: 10 pt, Not Bold
- Formatted: Font: 10 pt, Not Bold, Font color: Auto
- Formatted: Font: 10 pt, Not Bold, Font color: Auto
- Formatted: Font: 10 pt, Not Bold, Font color: Auto
- Formatted: Font: Not Bold



342 Figure 7: Downhole logging measurements performed along the TSM02 borehole (Scaglia Rossa Fm.). At the bottom: a detail  
343 of the structures intersected by the borehole.

Formatted: Font: 10 pt, Not Bold

Formatted: Font: 10 pt, Not Bold

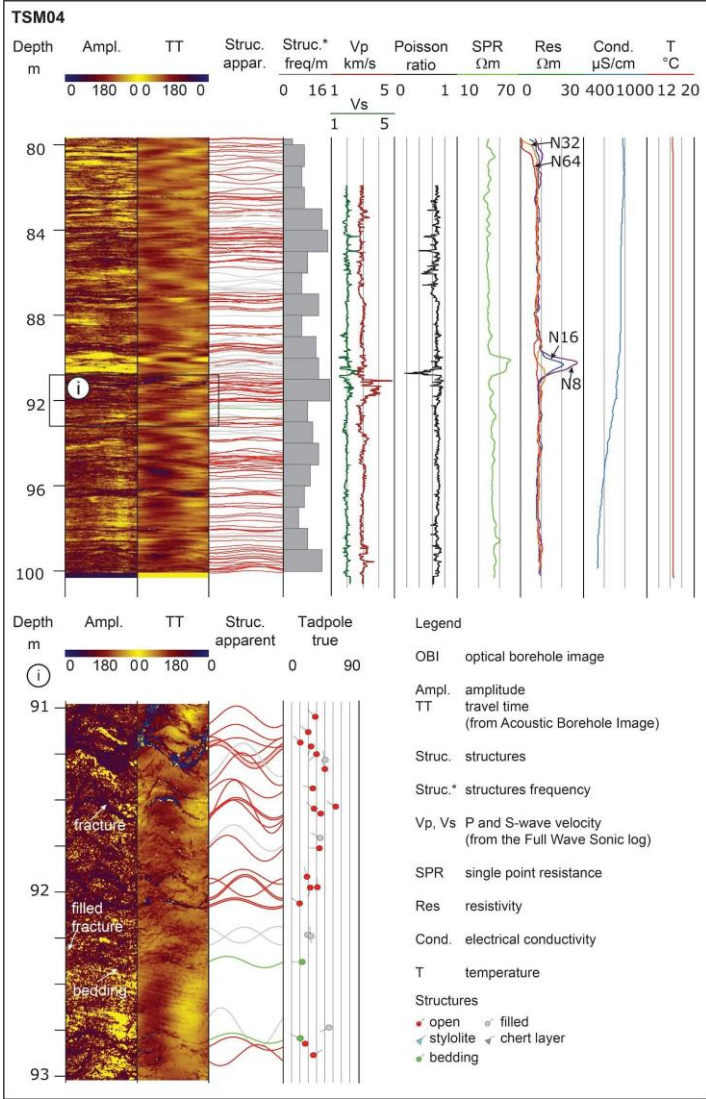
Formatted: Font: 10 pt, Not Bold

344  
345 TSM03. The poor quality of the OBI and ABI images made it difficult to perform a successful structural analysis. The unclear  
346 images are related to the high turbidity of the fluid in the borehole due to non-flushing of the borehole prior to acquisition and  
347 the high speed of running the OBI and ABI probes. Only the bedding planes were recognized showing a mean orientation of  
348 NW-SE (dip azimuth of N201°) with a very low dip of 11°. Owing to the low quality of the images, a geological survey was  
349 performed to measure bedding and main tectonic structures directly on the Marnoso-Arenacea outcrop near the drilling site  
350 (Fig. S2). Bedding varies from N204 near the borehole, to N167 and N155, dipping about 5-15°W, consistent with what was  
351 observed from the data analysis along the borehole. The thickness of the sandstone levels of Marnoso-Arenacea Fm. is up to  
352 100-120 cm, while the thickness of the grey marly layers ranges from 1 to 10 cm; they are laminated with cleavage planes sub-  
353 parallel to the bedding. There are fractures and sometimes sub-vertical faults, which are clearly visible in the sandstone layers,  
354 with an average fracture orientation of N050 sub-vertical, N215 sub-vertical faults with extensional displacement, N213  
355 dipping 76°W with left-lateral striae overlapped with oblique striae (pitch 55°, Fig. S2).

Formatted: Font: Not Bold

356 TSM04. The borehole intersected numerous discontinuity planes along the entire length of the measured log (Fig. 8). Although  
357 the log length is approximately only 20 m (79.8 to 100 m), the quality of the ABI images is significantly better compared to  
358 the TSM03 and TSM06 boreholes drilled in the same formation (Marnoso-Arenacea Fm.). The drastic decrease of cloudy fluid  
359 in the borehole is the combined result of wellbore flushing operations before starting log acquisition, and the low running  
360 speed of the ABI probe resulting in a good ABI image quality. 195 discontinuities between filled and open have been detected  
361 on image log with an average orientation of N184 and dipping never exceeding 60° (Fig. 10). In the field, upstream of the  
362 drilling site (Fig. S2), it was possible to measure bedding that is N180 oriented, dipping 25°W related to a small Late  
363 Cretaceous-Early Miocene outcrop of Tuscan turbidites (Fig. 2).

Formatted: Font: Not Bold



365 Figure 8: Downhole logging measurements performed along the TSM04 borehole (Marnoso-Arenacea Fm.). At the bottom: a  
366 detail of the structures intersected by the borehole. N means normal resistivity. The numbers [8, 16, 32 and 64] indicate the  
367 distance in inches between the electrode reference measuring point to the injection electrode in the resistivity sonde.

368  
369 TSM05. Analysis on OBI and ABI images allowed to clearly identify tectonic structures such as open and filled structures  
370 (Fig. 9). The bedding planes instead are dubious and difficult to recognize. Discontinuity planes show a spacing quite dense  
371 (12 planes per 1 m) up to 94.8 metres; below, they are very sparse, with sections of up to 3 m without discontinuity probably  
372 also due to the acquisition and to the presence of cloudy drilling fluid in the borehole. From the image analysis a total of 114  
373 planar structures have been identified with very consistent NW-SE orientation (corresponding to a dip azimuth of N219; Fig.  
374 10). From this dataset, we have marked at least 4 different categories of discontinuity according to their dip, the presence or  
375 absence of filling and their aperture. A first category of discontinuities is characterised by dip greater than 45° which is related  
376 to both open and filled fractures. They show planes approximately NW-SE oriented with dip both towards SW and towards  
377 NE. The filled fractures with dip less than 45° show a similar NW-SE trend as well as the open fracture zones including wider  
378 zones (decimetre thicknesses up to 1 m; Fig. 9-i) still have a NW-SE orientation and dips ranging from very low to almost  
379 vertical. The bedding planes are mainly sub-horizontal.

Formatted: Font: 10 pt, Not Bold

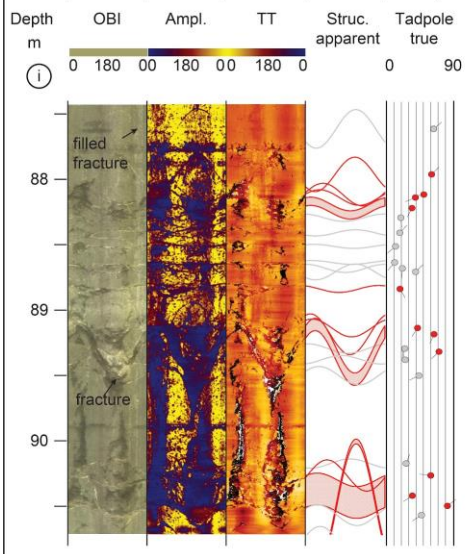
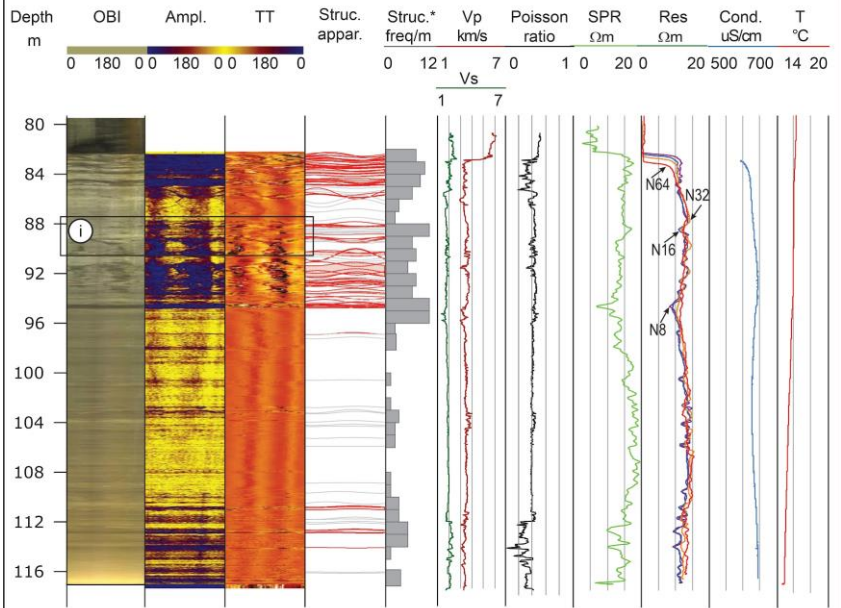
Formatted: Font: 10 pt, Not Bold, Font color: Auto

Formatted: Font: 10 pt, Not Bold

Formatted: Font: 10 pt, Not Bold

Formatted: Font: Not Bold

**TSM05**



- Legend**
- OBI optical borehole image
  - Ampl. amplitude
  - TT travel time (from Acoustic Borehole Image)
  - Struc. structures
  - Struc.\* structures frequency
  - Vp, Vs P and S-wave velocity (from the Full Wave Sonic log)
  - SPR single point resistance
  - Res resistivity
  - Cond. electrical conductivity
  - T temperature
- Structures**
- open
  - ◊ filled
  - ◀ stylolite
  - ◀ chert layer
  - ◊ bedding



381 [Figure 9](#): Downhole logging measurements performed along the TSM05 borehole (Schlier Fm.). At the bottom: a detail of the  
382 structures intersected by the borehole. [N](#) means normal resistivity. The numbers [8, 16, 32 and 64] indicate the distance in  
383 inches between the electrode reference measuring point to the injection electrode in the resistivity sonde.

384  
385 [TSM06](#). The structural analysis has been performed only on ABI image log allowing to identify 68 planar structures of which  
386 27 open and 41 filled in the Marnoso-Arenacea Fm. (Fig. 10). The planar discontinuities show a prevailing NE-SW orientation,  
387 and dip 20-30°W. There is also a minor NNW-SSE oriented data concentration characterised by steeper dip up to 60°NE. A  
388 weak zone oriented N300 dipping 54°NE with a width of about 21 cm, has also been identified along the TSM06 borehole. In  
389 the field very close to the drilling site, bedding is N190 oriented, dipping 30°W. In the surroundings, low angle bedding planes  
390 are also NW and NE oriented. Fracture planes are N125 oriented, dipping 88°S close to the drill; other high angle tectonic  
391 structures are also E-W and NE-SW (Fig. S2).

Formatted: Font: 10 pt, Not Bold

Formatted: Font: 10 pt, Not Bold

Formatted: Font: 10 pt, Not Bold

Formatted: Font: 10 pt, Not Bold

Formatted: Font: Not Bold

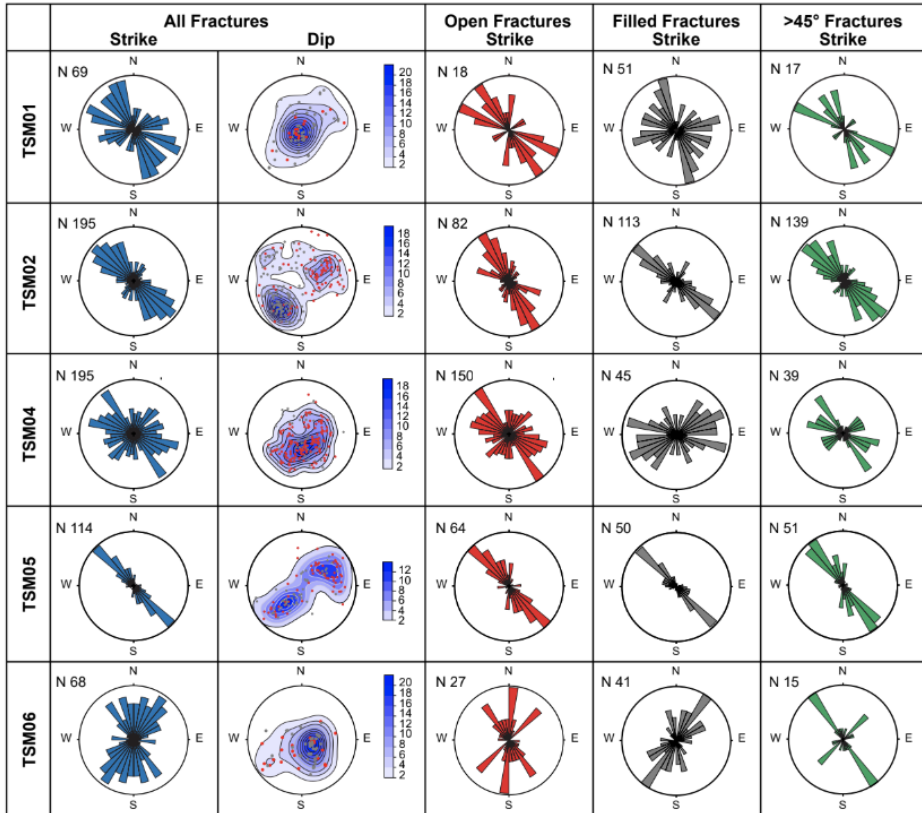


Figure 10. Rose diagrams and polar projections related to open and filled structures detected along the STAR boreholes (except TSM03). N: number of structures; DIP: poles of the planes (lower hemisphere) with the contouring (in percentage). The last column represents the fractures dipping >45°.

## 5 Discussion and Conclusion

In the framework of the STAR project, six shallow boreholes were drilled, conducting accurate geophysical downhole logs accurately, aimed to identify the most suitable depth in each borehole for the deployment of seismometers and strainmeters.

Formatted: Font: 10 pt, Not Bold, Font color: Auto

Formatted: Font: 10 pt, Not Bold

Formatted: Font: 10 pt, Not Bold, Font color: Auto

Formatted: Font: 10 pt, Not Bold

Formatted: Font: 10 pt, Not Bold, Font color: Auto

Formatted: Font: 10 pt, Not Bold

Formatted: Font: 10 pt, Not Bold, Font color: Auto

Formatted: Font: 10 pt, Not Bold

Formatted: Font: 10 pt, Not Bold

Formatted: Font: 10 pt, Not Bold

Formatted: Font: Not Bold, Font color: Auto

Formatted: Font: Not Bold, Font color: Auto

400 The results of the seismometer and strainmeter network will require more time to obtain useful information for the project  
401 itself, dedicated to the study of the brittle upper crust, and the structure and behaviour of the Alto Tiberina low-angle  
402 seismogenic normal fault, in particular. This paper pertains solely to the initial phase of the STAR project, specifically focusing  
403 on the analysis of downhole geophysical well logs.

404 Downhole logging was the only way to characterise the borehole section, allowing the physical and structural properties of  
405 each geological formation to be determined, due to the lack of core samples. These in situ measurements are sensitive to  
406 formation properties on a scale that is intermediate between those obtained from literature data analysis performed on core or  
407 outcrop samples and deep geophysical measurements, performed by exploration and production drilling companies. Most  
408 geophysical and petrophysical data available in the literature come either from rock samples, analysed in the laboratories, or  
409 from well-logs, acquired along deep wells, whereas our data from geophysical logging of shallow boreholes provides an almost  
410 untapped source of information.

#### 413 5.1 Physical properties

414 Regarding the calcareous formations of Maiolica and Scaglia Rossa Fms., crossed by the boreholes TSM01 and TSM02,  
415 respectively, the physical properties of these competent rock types are well reflected by the acquired log data (Table 1),  
416 showing low average GR values (less than 18 cps) and relatively high average values of  $V_p$  (5.3 and 4.9 km/s, respectively)  
417 and  $V_s$  (2.9 and 2.5 km/s, respectively). The almost pure limestones of the Maiolica Fm. are characterised by lower GR and  
418 higher  $V_p$  and  $V_s$  values, in comparison with the Scaglia Rossa Fm., where the clay content is significantly higher (up to 20%  
419 in the Tertiary upper portion of the Scaglia Fm., e.g. Arthur and Fischer, 1977).

420 The TSM03, TSM04, TSM05 and TSM06 boreholes were drilled in the marly intervals of the Neogene successions of the  
421 Marnoso-Arenacea Fm. and Schlier Fm. (TSM05). These clay-rich rocks are coherently characterised by high average GR  
422 (between 81 cps in the Schlier Fm. and 104 cps in the Marnoso-Arenacea Fm., TSM03) and low RES (between 9  $\Omega$ m and 29  
423  $\Omega$ m). The measurements include lower values for TSM04 (9  $\Omega$ m) and TSM05 (12  $\Omega$ m), Marnoso-Arenacea and Schlier  
424 respectively, intermediate values for TSM06 (18  $\Omega$ m), and higher values (up to 29  $\Omega$ m) for TSM03.

425 In greater detail, the average values are not totally representative of these complex formations, typically consisting of alternated  
426 marls and sandstones: similar suggestion derives from the relatively low  $V_p$  (3.0 to 3.5 km/s) and  $V_s$  (1.8 to ~2.0 km/s) values.  
427 The temperature recorded in the boreholes (Table 1) is rather constant with values between 12°C and 18°C without showing  
428 any significant variations related to e.g. outflow or inflow zones. Unfortunately, the shallow depth of the investigation limits  
429 the significance of the results.

430 We compared our RES results with two deep well data (San Donato 1 and Mt. Civitello 1 wells; <https://www.videpi.com>)  
431 drilled in the same formations and considering the same analysed depth interval, showing similar values between 20  $\Omega$ m and

Formatted: Font: Not Bold

30  $\Omega\text{m}$ , for the Marnoso-Arenacea Fm. (Fig. S3). We have also investigated the resistivity of the Schlier Fm. along the Canopo 1 well (<https://www.videpi.com>), although this latter is located far away from the study area, approximately 80 km NNE of Gubbio. Also in this case the resistivity values, around 7  $\Omega\text{m}$ , are comparable with our data (Fig. S3).

Information obtained from the velocity logs are more significant, including all 6 boreholes. We compared the Vp values recorded in the six shallow STAR boreholes (depth < 0.2 km, see Table 1) with data derived from sonic log analyses in much deeper wells (depth > 4 km) drilled in the same region for industrial purposes (Bigi et al., 2011; Scisciani et al., 2014; Montone and Mariucci, 2020; Trippetta et al., 2021). These studies report average Vp values between 4.0 km/s and 4.8 km/s for the Marnoso-Arenacea Fm., 4.4 km/s to 4.8 km/s for the Schlier Fm., 5.3 km/s to 5.8 km/s for the Scaglia Rossa Fm., and 5.5 km/s to 6.1 km/s for the Maiolica Fm. All these values are approximately 15% higher than our results but follow the same overall trend, with higher average Vp values recorded in the Maiolica and lower values in the Tertiary marly Formations. This increase in P-wave velocity with depth is primarily attributed to increased rock density and compaction, particularly in the Tertiary formations.

Due to a different degree of porosity linked to the different investigated depths and to the pore type, P-wave velocity can significantly change (e.g. Hairabian et al., 2014; Smeraglia et al., 2014; Trippetta et al., 2021). Moreover, P-wave velocity also depends on factors such as lithology changes, presence of fractures or faults and also on the different amount of tectonic deformation observed in different structural domains (Trippetta et al., 2021). Collecting and analysing the velocity data of upper crustal sedimentary rocks is very useful under different aspects. On one end, these values help ~~in~~ building ~~up~~ and calibrating more accurate, 2D and 3D velocity models, that can be used for improving the earthquakes localization (e.g. Latorre et al., 2016; Montone and Mariucci, 2023) as well as to constrain depth conversion of seismic reflection profiles. On the other hand, since the velocity parameters of rocks are strictly related to their rigidity, velocity values also reflect ~~into~~ their different mechanical behaviour and may ultimately influence earthquake generation and distribution. In our case, the more competent carbonate formations (i.e. Maiolica and Scaglia Rossa Fms.) are characterised by systematically higher velocities ~~ty~~ ~~values~~ ~~compared to~~ ~~with respect to the~~ less competent, clay-rich turbidite formations (i.e. Schlier and Marnoso-Arenacea Fms.).

In the ATF region, as well as in adjacent areas in the same seismotectonic framework of the Central Apennines, several recent studies of the relationships between seismicity distribution and upper crustal geological setting have been recently performed, by plotting accurately relocated seismic sequences on well-calibrated geological subsurface models, based on depth conversion of seismic reflection profiles (e.g. Latorre et al., 2016; Barchi et al., 2021; Collettini et al., 2022; Chiaraluce et al., 2017b). These studies coherently indicated that upper crustal seismicity (and the normal faulting earthquake mainshocks, in particular) are systematically hosted in the high velocity, Mesozoic or Early Tertiary successions, consisting of carbonates, dolostones and anhydrites, whilst only few, low magnitude events are recorded in the overlying, less competent Neogene turbidites, mainly consisting of marls and sandstones.

Formatted: Not Highlight

464 5.2 Stress Field

465 To constrain the orientation of the stress field in the area of the STAR project, we have analysed and interpreted the fractures  
466 detected in the six boreholes and compared them with the breakout orientations from the two deep wells and also with the  
467 other stress indicators, mainly focal mechanism data. In our boreholes, ABI and OBI images do not reveal any borehole  
468 breakouts. However, breakouts at very shallow depth could not be related or representative to the stress field because their  
469 occurrence would be linked to local effects such as topography, local faulting, folding, and other near-surface geological  
470 structures. As already mentioned, in the STAR study area (Fig. 2) two deep wells (SD and MC) were drilled in the past,  
471 reaching a depth of 4763 and 5600 m, respectively. The SD well is located very close to the ATF, intersecting it at a shallow  
472 depth; while the MC well, approximately 15 km east of the ATF fault, intersects additional tectonic structures. A thorough  
473 analysis of borehole breakout stress data conducted along the two deep wells, allowed to deduce the current stress field  
474 orientation (Mariucci et al., 2008). In the case of the SD well, the borehole breakout results reveal a minimum horizontal stress  
475 orientation of  $N055\pm 22^\circ$ ; the MC well exhibits a slightly different stress orientation, with a value of  $N012\pm 29^\circ$  (Fig. 11).

Formatted: Font: Not Bold

Formatted: Font: Not Bold

Formatted: Font: Not Bold

Formatted: Font: Not Bold

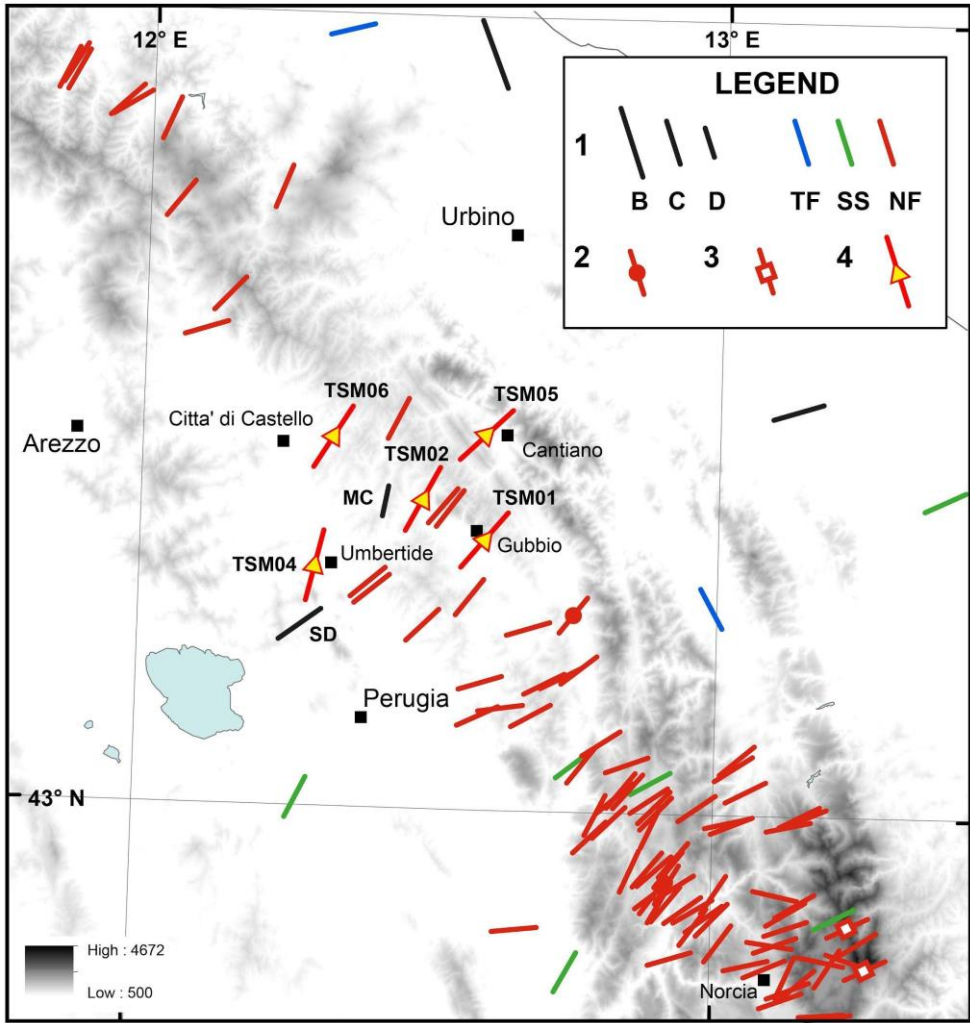
Formatted: Font: Not Bold

Formatted: Font: Not Bold

Formatted: Font: Not Bold

Formatted: Font: Not Bold

Formatted: Font: Not Bold



478 **Figure 11**; Present-day stress field of Central Italy. The minimum horizontal stress orientations inferred both from the >45°  
479 dipping fractures detected along the STAR boreholes (bars with yellow triangles) and from the Italian Present-day Stress  
480 Indicators database IPSI 1.6 (Mariucci and Montone, 2024) are shown. 1- Borehole breakout (black bar) and focal mechanism  
481 (coloured bar) data; 2- formal inversion data; 3- fault data. All data are scaled by quality (from B to D) and coloured according  
482 to tectonic regime: black bar is unknown regime (breakout), blue is thrust faulting, green is strike-slip faulting, red is normal  
483 faulting. 4- data from TSM boreholes. 1— Stress data scaled by quality (from B to D) and coloured according to tectonic regime:  
484 black bar is unknown regime (borehole breakout data), blue is thrust faulting, green is strike-slip faulting, red is normal  
485 faulting; 2- formal inversion data; 3- fault data; 4- data from TSM boreholes.

486  
487 To interpret the structural data obtained along the STAR boreholes, we have considered i) the shallow depth of the boreholes,  
488 ii) their near-vertical inclination, that strongly underestimates occurrence of near-vertical features (Terzaghi, 1965; Massiot et  
489 al., 2015), and iii) the difficulty in distinguishing fractures from faults in this type of data.

490 Along the STAR boreholes, the main features with a dip angle > 45° (Fig. 10, column f) show a predominantly NW-SE  
491 orientation and could be interpreted as pre-existing fractures generated in the early phases of the deformation history before  
492 folding (Price, 1966).

493 Considering that the current stress field in the area is primarily due to an extensional regime, with the main compressional  
494 stress, sigma 1, vertical and horizontal sigma 3 NE-SW oriented, the tectonic structures associated with this latter stress field  
495 consequently develop normal faults and high-dip extensional fractures. These > 45° NW-SE structures, favourably oriented  
496 with respect to the current extensional stress field (Fig. 11), might have been reactivated as extensional fractures. In TSM04  
497 and TSM06 boreholes, for structures with a dip greater than 45° (Fig. 10, column f), another orientation is also observed,  
498 approximately 90° from the previous one. We can assume that both fractures NW-SE and NE-SW oriented are  
499 contemporaneous and linked to the same extensional stress field, primarily guided by a vertical sigma 1. On the other hand,  
500 structures with low dip - still NW-SE oriented - could be attributed to previous compressive deformation phases linked to a  
501 stress field characterised by a horizontal sigma 1, oriented NE-SW. Taking into careful consideration the different depths  
502 investigated by the STAR boreholes (<0.2 km) with respect to the active stress data mainly inferred from breakout data in deep  
503 wells (0.5-6 km) and focal mechanisms of crustal earthquakes (usually 5-15 km), we can still compare their results (Fig. 11).  
504 In fact, most of the results from literature on the orientation of the stress field have shown that different crustal depths do not  
505 reorient or change the stress field (Heidbach et al., 2016; Mariucci and Montone, 2024). An almost constant orientation of the  
506 minimum horizontal stress characterises this sector of the Apennines, from the southern L'Aquila and Norcia zones to the areas  
507 north of Gubbio, showing only a slight rotation from ENE-NE directions to NE-NNE directions, respectively (Fig. 11). This  
508 is observed from numerous data derived from earthquake focal mechanisms as well as breakout data in deep wells, also present  
509 in the southernmost sector (Mariucci and Montone, 2016) and active fault data (Lavecchia et al., 2022), under a stress regime  
510 that can be defined as exclusively extensional.

511 In conclusion, our paper provides reliable values on physical properties of rocks, in particular P-wave velocity, which can be  
512 used to characterise crustal velocity models and allow detailed interpretation of seismic profiles, investigating the first two

Formatted: Font: 10 pt, Not Bold, Font color: Auto

Formatted: Font: 10 pt, Not Bold

Formatted: Font: 10 pt, Not Bold, Font color: Auto

Formatted: Font: 10 pt, Not Bold

Formatted: Font: 10 pt, Not Bold, Font color: Auto

Formatted: Font: 10 pt, Not Bold

Formatted: Font: 10 pt, Not Bold, Font color: Auto

Formatted: Font: 10 pt, Not Bold, Font color: Auto

Formatted: Font: 10 pt, Not Bold, Font color: Auto

513 hundred metres of the crust. [However, detailed geophysical measurements from shallow boreholes are relatively rare. A small,](#)  
514 [homogeneous rock sample analysed in the laboratory may not accurately represent the complexity of the in situ rock formation,](#)  
515 [which can exhibit significant internal variability in composition and fracturing. Additionally, although our sites provide in situ](#)  
516 [measurements, they represent a relatively small dataset compared to the extensive data collected from deep well logs, which](#)  
517 [span hundreds of metres. This limitation could explain the discrepancies observed, such as the differences in Vp values. While](#)  
518 [our measured values are lower than the average data, they still fall within the acceptable range.](#)  
519 [Beyond the specific case presented, our data significantly enhance our understanding of the upper crust. These in situ](#)  
520 [measurements bridge the gap between data from outcropping rocks and data from deeper wells. In particular, this scientific](#)  
521 [approach is able to provide useful geophysical information at the very shallow crustal depth \(<0.2 km\), typically not explored](#)  
522 [by either the scientific community or oil and gas industry. Our study demonstrates that even a limited dataset can provide](#)  
523 [valuable insights and represent possible case history for future projects. With an expanded dataset across a region of interest,](#)  
524 [it would be possible to illuminate a comprehensive section of the crust, extending from the surface to several kilometres deep,](#)  
525 [and potentially even deeper.](#)

Formatted: Font: (Default) Arial, 11 pt, Font color: Black

## 527 **References**

- 528 Amato, A. and Cocco, M. (eds): The Umbria-Marche, central Italy, Seismic Sequence of 1997–1998, *Journal of Seismology*,  
529 4(4), 5–598, 2000.
- 530 Amato, A., Azzara, R., Chiarabba, C., Cimini, G. B., Cocco, M., Di Bona, M., Margheriti, L., Mazza, S., Mele, F., Selvaggi, G.,  
531 Basili, A., Boschi, E., Courboux, F., Deschamps, A., Gaffet, S., Bittarelli, G., Chiaraluca, L., Piccinini, D., and Ripepe, M.:  
532 The 1997 Umbria-Marche seismic sequence: a first look at the main shocks and aftershocks, *Geophysical Research Letters*, 25,  
533 2861–2864, 1998.
- 534 [Anderlini, L., Serpelloni, E., and Belardinelli, M.: Creep and locking of a low-angle normal fault: Insights from the Altotiberina](#)  
535 [fault in the Northern Apennines \(Italy\), \*Geophysical Research Letters\*, 43, 4321–4329, <https://doi.org/10.1002/2016GL068604>,](#)  
536 [2016.](#)
- 537 Arthur, M. A. and Fischer, A. G.: Upper Cretaceous-Paleocene magnetic stratigraphy at Gubbio, Italy I. Lithostratigraphy and  
538 sedimentology, *Geological Society of American Bulletin.*, 88, 367–371, 1977.
- 539 Barchi, M. R., De Feyter, A., Magnani, M.B., Minelli, G., Pialli, G. and Sotera, B. M.: The structural style of the Umbria-Marche  
540 fold and thrust belt, *Memorie della Società Geologica Italiana*, 52, 557–578, 1998.
- 541 Barchi, M. R., Carboni, F., Michele, M., Ercoli, M., Giorgetti, C., Porreca, M., Azzaro, S., Chiaraluca, L.: The influence of  
542 subsurface geology on the distribution of earthquakes during the 2016-2017 Central Italy seismic sequence, *Tectonophysics*,  
543 807, 22879, <https://doi.org/10.1016/j.tecto.2021.228797>, 2021.



544 Barchi, M. R. and Collettini, C.: Seismicity of central Italy in the context of the geological history of the Umbria-Marche  
545 Apennines, *Special Paper of the Geological Society of America*, 542, 175 – 190, 2019.

546 Barchi, M. R. and Mirabella, F.: The 1997-98 Umbria-Marche earthquake sequence: "Geological" vs. "seismological" faults,  
547 *Tectonophysics*, 476(1-2), 170-179, 10.1016/j.tecto.2008.09.013 (2009).

548 Barchi, M. R.: The Neogene-Quaternary evolution of the Northern Apennines: crustal structure, style of deformation and  
549 seismicity, *Journal of the Virtual Explorer*, 36, 2010.

550 Bigi, S., Casero, P., and Ciotoli, G.: Seismic interpretation of the Laga basin: constraints on the structural setting and kinematics  
551 of the Central Apennines, *Journal of Geological Society of London*, 168, 179–190, <https://doi.org/10.1144/0016-76492010-084>,  
552 2011.

553 Bohnhoff, M., Dresen, G., Ceken, U., Kadirioglu, F. T., Kartal, R. F., Kilic, T., Nurlu, M., Yanik, K., Acarel, D., Bulut, F.,  
554 Kloth, A., Johnson, W., Malin, P. and Mencin, D.: GONAF – the borehole Geophysical Observatory at the North Anatolian  
555 Fault in the eastern Sea of Marmara, *Scientific Drilling: reports on deep earth sampling and monitoring*, 22, 19-28,  
556 <https://doi.org/10.5194/sd-22-19-2017>, 2017.

557 Boncio, P. and Lavecchia, G.: A geological model for the Colfiorito earthquakes (September–October 1997, central Italy),  
558 *Journal of Seismology*, 4, 345–356, 2000.

559 Boncio, P., Pizzi, A., Brozzetti, F., Pomposo, G. Lavecchia, G., Di Naccio, D., Ferrarini, F.: Coseismic ground deformation of  
560 the 6 April 2009 L'Aquila earthquake (central Italy, Mw6.3), *Geophysical Research Letters*, 37, L06308, 2010.

561 Caricchi, C., Aldega, L., Barchi, M. R., Corrado, S., Grigo, D., Mirabella, F., Zattin, M.: Exhumation patterns along shallow  
562 low-angle normal faults: an example from the Altotiberina active fault system (Northern Apennines, Italy), *Terra Nova*, 27, 312–  
563 321, <https://doi.org/doi:10.1111/ter.12163>, 2015.

564 Cello, G., Mazzoli, S., Tondi, E., and Turco, E.: Active tectonics in the central Apennines and possible implications for seismic  
565 hazard analysis in peninsular Italy, *Tectonophysics*, 272, 43–68, [http://dx.doi.org/10.1016/S0040-1951\(96\)00275-2](http://dx.doi.org/10.1016/S0040-1951(96)00275-2), 1997.

566 Chiarabba, C., De Gori, P., Cattaneo, M., Spallarossa, D., and Segou, M.: Faults geometry and the role of fluids in the 2016-  
567 2017 Central Italy seismic sequence, *Geophys. Res. Lett.*, 45, 6963–6971, <https://doi.org/10.1029/2018GL077485>, 2018.

568 Chiarabba, C., Jovane, L., and Di Stefano, R.: A new view of Italian seismicity using 20 years of instrumental recordings,  
569 *Tectonophysics*, 305, 251–268, 2005.

570 Chiaraluce, L., Di Stefano, R., Tinti, E., Scognamiglio, L., Michele, M., Casarotti, E., Cattaneo, M., De Gori, P., Chiarabba, C.,  
571 Monachesi, G., Lombardi, A., Valoroso, L., Latorre, D., Marzorati, S.: The 2016 Central Italy seismic sequence: a first look at  
572 the mainshocks, aftershocks, and source models, *Seismological Research Letters*, 88(3), 757–771,  
573 <https://doi.org/10.1785/0220160221>, 2017b.

574 Chiaraluce, L., Amato, A., Carannante, S., Castelli, V., Cattaneo, M., Cocco, M., Collettini, C., D'Alema, E., Di Stefano, R.,  
575 Latorre, D., Marzorati, S., Mirabella, F., Monachesi, G., Piccinini, D., Nardi, A., Piersanti, A., Stramondo, S., and Valoroso, L.:

576 The Alto Tiberina Near Fault Observatory (northern Apennines, Italy), *Annals of Geophysics*, 57, S0327,  
577 <https://doi.org/10.4401/ag-6426>, 2014a.

578 Chiaraluze, L., Festa, G., Bernard, P., Caracausi, A., Carliccio, I., Clinton, J., Di Stefano, R., Elia, L., Evangelidis, C., Ergintav,  
579 S., Jianu, O., Kaviris, G., Marmureanu, A., Sebelă, S., and Sokos, E.: The Near Fault Observatory community in Europe: a new  
580 resource for faulting and hazard studies, *Annals of Geophysics*, 65(3), <https://doi.org/10.4401/ag-8778>, 2022.

581 Chiaraluze, L., Festa, G., Bernard, P., Caracausi, A., Carluccio, I., Clinton, J.F., Di Stefano, R., Elia, L., Evangelidis, C.P.,  
582 Ergintav, S., Jianu, O., Kaviris, G., Marmureanu, A., Šebela, S., and Sokos, E.: The role of rheology, crustal structures and  
583 lithology in the seismicity distribution of the northern Apennines, *Tectonophysics*, 694, 280–291.  
584 <https://doi.org/10.1016/j.tecto.2016.11.011>, 2017a.

585 Chiaraluze, L., Colletini, C., Cattaneo, M., and Monachesi, G.: The shallow boreholes at the Altotiberina near fault Observatory  
586 (TABOO; northern Apennines of Italy), *Scientific Drilling*, 17, 31–35, <https://doi.org/10.5194/sd-17-31-2014>, 2014b.

587 Chiaraluze, L., Ellsworth, W. L., Chiarabba, C., and Cocco, M.: Imaging the complexity of an active normal fault system: The  
588 1997 Colfiorito (Central Italy) case study, *Journal of Geophysical Research*, 108(B6), <https://doi.org/10.1029/2002JB002166>,  
589 2003.

590 [Chiaraluze, L., Bennett, R., Mencin, D., Johnson, W., Barchi, M.R., Bohnhoff, M., Baccheschi, P., Caracausi, A., Calamita, C.,  
591 Cavaliere, A., Gualandri, A., Mandler, E., Mariucci, M.T., Martelli, L., Marzorati, S., Montone, P., Pantaleo, D., Pucci, S.,  
592 Serpelloni, E., Supino, M., Stramondo, S., Hanagan, C., Van Boskirk, L., Gottlieb, M., Mattioli, G., Urbani, M., Mirabella, F.,  
593 Akimbekova, A., Pierdominici, S., Wiersberg, T., Chris Marone, C., Palmieri, L., and Schenato, L.: A Strainmeter Array as  
594 Fulcrum of Novel Observatory Sites Along the Alto Tiberina Near Fault Observatory, \*Scientific Drilling\*, 33, 173-190,  
595 <https://doi.org/10.5194/sd-33-173-2024>, 2024.](#)

596 Ciaccio, M.G., Barchi, M.R., Chiarabba, C., Mirabella, F., and Stucchi, E.: Seismological, geological and geophysical constraints  
597 for the Gualdo Tadino fault, Umbria–Marche Apennines (central Italy), *Tectonophysics*, 406(3-4), 233-247,  
598 <https://doi.org/10.1016/j.tecto.2005.05.027>, 2005.

599 Cinti, F. R., Cucci, L., Marra, F., and Montone, P.: The 1997 Umbria-Marche (Italy) earthquake sequence: Relationship between  
600 ground deformation and seismogenic structure, *Geophysical Research Letters*, 26, 895–898, 1999.

601 Colletini, C., Barchi, M. R., De Paola, N., Trippetta, F., and Tinti, E.: Rock and fault rheology explain differences between on  
602 fault and distributed seismicity, *Nature communication*, 13, 5627, <https://doi.org/10.1038/s41467-022-33373-y>, 2022.

603 Cresta, S., Monechi, S., and Parisi, G.: Stratigrafia del Mesozoico al Cenozoico nell'area Umbro-Marchigiana, *Memorie  
604 Descrittive della Carta Geologica d'Italia*, 34, 185, 1989.

605 Davatzes, N.C. and Hickman, S.H.: Stress, fracture, and fluid-flow analysis using acoustic and electrical image logs in hot  
606 fractured granites of the Coso geothermal field, California, U.S.A., in M. Poppelreiter, C. Garcia-Carballido, and M. Kraaijveld,  
607 eds., *Dipmeter and borehole image log technology*. AAPG Memoir 92, p. 259 – 293, 2010.

608 De Paola, N., Faulkner, D.R., and Colletti, C.: [Brittle versus ductile deformation as the main control on the transport properties](#)  
609 [of low-porosity anhydrite rocks](#)~~Localized versus distributed deformation as a control on the evolution of permeability in~~  
610 [anhydrite rocks](#), *Journal of Geophysical Research*, 114, B06211, <http://dx.doi.org/10.1029/2008JB005967>, 2009.

611 Deschamps, A., Iannaccone, G., and Scarpa, R.: The Umbrian earthquake (Italy) of 19 September 1979, *Annales Geophysicae*,  
612 2(1), 29-36, 1984.

613 Diaferia, I., Barchi, M., Loddo, M., Schiavone, D., and Siniscalchi, A. Detailed imaging of tectonic structures by multiscale  
614 Earth resistivity tomographies: The Colfiorito normal faults (central Italy). *Geophys. Res. Lett.*, 33, L09305,  
615 doi:10.1029/2006GL025828, 2006

616 Ellis D.V. and Singer J.M.: *Well Logging for Earth Scientists*. 2nd edition Springer, pp 699, 2007.

617 EMERGEO Working Group: Evidence for surface rupture associated with the Mw 6.3 L'Aquila earthquake sequence of April  
618 2009 (central Italy), *Terra Nova*, 22, 43–51, 2010.

619 Fischer, T., Hrubcová, P., Dahm, T., Woith, H., Vylita, T., Ohrnberger, M., Vlček, J., Horálek, J., Dedeček, P., Zimmer, M.,  
620 Lipus, M., Pierdominici, S., Kallmeyer, J., Krüger, F., Hannemann, K., Korn, M., Kämpf, H., Reinsch, T., Klicpera, J., Volmer,  
621 D., Daskalopoulou, K. (2022). ICDP Eger Rift observatory: Magmatic Fluids Driving the Earthquake Swarms and Deep  
622 Biosphere - Scientific and technological achievements, *Scientific Drilling*, 31, 31-49, <https://doi.org/10.5194/sd-31-31-2022>

623 Haessler, H., Gaulon, R., Rivera, L., Console, R., Frogneux, M., Gasparini, G., Martel, L., Patau, G., Siciliano, M., and Cisternas,  
624 A.: The Perugia (Italy) earthquake of 29 April 1984: a microearthquake survey, *Bulletin of the Seismological Society of America*,  
625 78, 1948–1964, 1988.

626 Hairabian, A., Fournier, F., Borgomano, J., and Nardon, S.: Depositional facies, pore types and elastic properties of deep-water  
627 gravity flow carbonates *Journal of Petroleum Geology*, 37, 231–249, 2014.

628 Heidbach, O., Rajabi, M., Reiter, K., Ziegler, M., and WSM Team: World Stress Map Database Release 2016. V. 1.1, GFZ Data  
629 Services, <https://doi.org/10.5880/WSM.2016.001>, 2016.

630 Italian CMT dataset (<http://www.bo.ingv.it/RCMT/Italydataset.html>)

631 Langbein, J., Murray, J.R., and Snyder, H.A.: Coseismic and initial postseismic deformation from the 2004 Parkfield, California,  
632 earthquake, observed by Global Positioning System, electronic distance meter, creepmeters, and borehole strainmeters, *Bulletin*  
633 *of the Seismological Society of America*, 96(4B), S304-S320, 2006.

634 Latorre, D., Mirabella, F., Chiaraluca, L., Trippetta, F., and Lomay, A.: Assessment of earthquake locations in 3-D deterministic  
635 velocity models: A case study from the Altotiberina Near Fault Observatory (Italy), *Journal of Geophysical Research: Solid*  
636 *Earth*, 121(11), 8113-8135, <https://doi.org/10.1002/2016JB013170>, 2016.

637 Lavecchia, G., Adinolfi, G. M., de Nardis, R., Ferrarini, F., Cirillo, D., Brozzetti, F., De Matteis, R., Festa, G., and Zollo, A.:  
638 Multidisciplinary inferences on a newly recognized active east-dipping extensional system in Central Italy, *Terra Nova*, 29, 77–  
639 89, 2017.

640 Lavecchia, G., Bello, S., Adrenacci, C., Cirillo, D., Ferrarini, F., Vicentini, N., de Nardis, R., Roberts, G., Brozzetti, F.:  
641 Quaternary fault strain INDicators database - QUIN 1.0-first release from the Apennines of central Italy, *Scientific Data*, 9(1),  
642 doi 10.1038/s41597-022-01311-8, 2022.

643 Mariucci M.T. and Montone P.: Contemporary stress field in the area of the 2016 Amatrice seismic sequence (central Italy),  
644 *Annals of Geophysics*, 59, fast track 5, doi:10.4401/ag-7235, 2016.

645 Mariucci M.T., Montone P., and Pierdominici S.: Active stress field in central Italy: a revision of deep well data in Umbria  
646 region, *Annals of Geophysics*, 51, 2/3, 433-442, 2008.

647 Mariucci, M.T. and Montone, P.: IPSI 1.6, Database of Italian Present-day Stress Indicators, Istituto Nazionale di Geofisica e  
648 Vulcanologia (INGV), <http://doi.org/10.13127/IPSI.1.6>, 2024.

649 Marzorati, S., Massa, M., Cattaneo, M., Monachesi, G., and Frapiccini, M.: Very detailed seismic pattern and migration inferred  
650 from the April 2010 Pietralunga (northern Italian Apennines) micro-earthquake sequence, *Tectonophysics*, 610, 91–109,  
651 <https://doi.org/10.1016/j.tecto.2013.10.014>, 2014.

652 Massiot, C., McNamara, D., and Lewis, B.: Processing and analysis of high temperature geothermal acoustic borehole image  
653 logs in the Taupo Volcanic Zone, New Zealand, *Geothermics*, 53, 190–201, <https://doi.org/10.1016/j.geothermics.2014.05.010>,  
654 2015.

655 [Mcginnis, R. N., Ferrill, D. A., Morris, A. P., Smart, K. J. and Lehrmann, D.: Mechanical stratigraphic controls on natural](#)  
656 [fracture spacing and penetration. \*Journal of Structural Geology\*, 95, 160–170. <https://doi.org/10.1016/j.jsg.2017.01.001>, 2017.](#)

657 [Medici, G, Ling F., and Shang, J.: Review of discrete fracture network characterization for geothermal energy extraction.](#)  
658 [Frontiers Earth Science, 11, 1328397. <https://doi.org/10.3389/feart.2023.1328397>, 2023.](#)

659 Michele, M., Chiaraluca, L., Di Stefano, R., and Waldhauser, F.: Fine-Scale Structure of the 2016–2017 Central Italy Seismic  
660 Sequence From Data Recorded at the Italian National Network, *Journal of Geophysical Research*, 125, e2019JB01844,  
661 <https://doi.org/10.1029/2019JB018440>, 2020.

662 Mildon, Z. K., Roberts, G. P., Faure Walker, J. P., Wedmore, L. N. J., and McCaffrey, K. J. W.: Active normal faulting during  
663 the 1997 seismic sequence in Colfiorito, Umbria: Did slip propagate to the surface?, *Journal of Structural Geology*, 91, 102–  
664 113, 2016.

665 Mirabella, F., Brozzetti, F., Lupattelli, A., and Barchi, M.R.: Tectonic evolution of a low-angle extensional fault system from  
666 restored cross-sections in the Northern Apennines (Italy), *Tectonics*, 30, TC6002, doi:10.1029/2011TC002890, 2011.

667 Mirabella, F., Ciaccio, M.G., Barchi, M.R., and Merlini, S.: The Gubbio normal fault (Central Italy): geometry, displacement  
668 distribution and tectonic evolution, *Journal of Structural Geology*, 26, 2233-2249, doi:10.1016/j.jsg.2004.06.009, 2004.

669 Montone, P. and Mariucci, M. T.: The new release of the Italian contemporary stress map, *Geophysical Journal International*,  
670 205, 1525–1531, <https://doi.org/10.1093/gji/ggw100>, 2016.

671 Montone, P. and Mariucci, M.T.: Constraints on the Structure of the Shallow Crust in Central Italy from Geophysical Log Data,  
672 *Scientific Reports*, 10, 3834, <https://doi.org/10.1038/s41598-020-60855-0>, 2020.

673 Montone, P. and Mariucci M.T.: Lateral Variations of P-Wave Velocity from Deep Borehole Data in the Southern Apennines,  
674 Italy, *Pure and Applied Geophysics*, 180, 1925–1944, <https://doi.org/10.1007/s00024-023-03248-4>, 2023.

675 Pierdominici, S. and Kück, J.: Borehole Geophysics. In: *Encyclopedia of Geology (Second Edition)*, Elsevier, 746–760,  
676 <https://doi.org/10.1016/B978-0-08-102908-4.00126-0>, 2021.

677 Pierdominici, S., Millett, J. M., Kück, J. K. M., Thomas, D., Jerram, D. A., Planke, S., Haskins, E., Lautze, N., and Galland, O.:  
678 Stress field interactions between overlapping shield volcanoes: Borehole breakout evidence from the island of Hawaii, USA,  
679 *Journal of Geophysical Research*, 125, e2020JB019768, <https://doi.org/10.1029/2020JB019768>, 2020.

680 Pizzi, A., Di Domenica, A., Gallovic, F., Luzi, L., and Puglia, R.: Fault segmentation as constraint to the occurrence of the main  
681 shocks of the 2016 Central Italy seismic sequence, *Tectonics*, 36, 2370–2387, <https://doi.org/10.1002/2017TC004652>, 2017.

682 Pondrelli, S. and Salimbeni, S.: Italian CMT Dataset (Data set). Istituto Nazionale di Geofisica e Vulcanologia (INGV),  
683 <https://doi.org/10.13127/rcmt/italy>, 2006.

684 Pondrelli, S., Salimbeni, S., Ekström, G., Morelli, A., Gasperini, P., and Vannucci, G.: The Italian CMT dataset from 1977 to  
685 the present, *Physics of the Earth and Planetary Interiors*, 159(3-4), 286–303, doi:10.1016/j.pepi.2006.07.008, 2006.

686 Porreca, M., Minelli, G., Ercoli, M., Brobia, A., Mancinelli, P., Cruciani, F., Giorgetti, C., Carboni, F., Mirabella, F., Cavinato,  
687 G., Cannata, A., Pauselli, C., and Barchi, M. R.: Seismic reflection profiles and subsurface geology of the area interested by the  
688 2016–2017 earthquake sequence (Central Italy), *Tectonics*, 37, 1116–1137, <https://doi.org/10.1002/2017TC004915>, 2018.

689 Price, N.J. *Fault and Joint Development in Brittle and Semi-Brittle Rocks*. Pergamon Press, Oxford, 1966 *Quick Regional*  
690 *Moment Tensors*, <http://autorcmt.bo.ingv.it/quicks.html>

691 Rider, M.H. and Kennedy, M.: *The Geological Interpretation of Well Logs*, 432 pp, Rider-French, Scotland, 2011.

692 Schön, J.H.: *Physical Properties of Rocks - Fundamentals and Principles of Petrophysics*. 2nd Edition -Elsevier, 2015.

693 Scisciani, V., Agostini, S., Calamita, F., Pace, P., Cilli, A., Giori, I., and Paltrinieri, W.: Positive inversion tectonics in foreland  
694 fold-and thrust belts: a reappraisal of the Umbria–Marche northern Apennines (Central Italy) by integrating geological and  
695 geophysical data, *Tectonophysics*, 637, 218–237, <https://doi.org/10.1016/j.tecto.2014.10.010>, 2014.

696 Serra, O.: *Fundamentals of well-log interpretation. Part I: The acquisition of logging data*. *Developments in petroleum science*  
697 15A, Amsterdam, Elsevier, pp 435, 1984.

698 Smeraglia, L., Trippetta, F., Carminati, E., and Mollo, S.: Tectonic control on the petrophysical properties of foredeep sandstone  
699 in the Central Apennines, Italy, *Journal of Geophysical Research*, 119, 9077–9094, 2014.

700 Terzaghi, R. D.: Sources of error in joint surveys, *Geotechnique*, 15(3), 287–304, <https://doi.org/10.1680/geot.1965.15.3.287>,  
701 1965.

702 Tinti, E., Scognamiglio, L., Michelini, A., and Cocco, M.: Slip heterogeneity and directivity of the ML 6.0 2016 Amatrice  
703 earthquake estimated with rapid finite-fault inversion, *Geophysical Research Letters*, 43(10), 10,745–10,752,  
704 <https://doi.org/10.1002/2016GL071263>, 2016.

705 Trippetta F., Barchi, M. R., Tinti, E., Volpe, G., Rosset, G., and De Paola, N.: Lithological and stress anisotropy control  
706 large-scale seismic velocity variations in tight carbonates, *Scientific Reports*, 11, 9472, [https://doi.org/10.1038/s41598-021-](https://doi.org/10.1038/s41598-021-89019-4)  
707 89019-4, 2021.

708 Trippetta, F., Collettini, C., Vinciguerra, S., and Meredith, P.G.: Laboratory measurements of the physical properties of Triassic  
709 evaporites from central Italy and correlation with geophysical data, *Tectonophysics*, 492, 121–132,  
710 <http://dx.doi.org/10.1016/j.tecto.2010.06.001>, 2010.

711 Valoroso, L., Chiaraluca, L., Di Stefano, R., and Monachesi, G.: Mixed-mode slip behaviour of the Altotiberina low-angle  
712 normal fault system (Northern Apennines, Italy) through high-resolution earthquake locations and repeating events, *Journal of*  
713 *Geophysical Research: Solid Earth*, 122, <https://doi.org/10.1002/2017JB014607>, 2017.

714 Valoroso, L., Chiaraluca, L., Piccinini, D., Di Stefano, R., and Waldhauser, F.: Radiography of a normal fault system by 64,000  
715 high-precision earthquake locations: The 2009 L'Aquila (central Italy) case study, *Journal of Geophysical Research: Solid Earth*,  
716 118, 1156–1176, <https://doi.org/10.1002/jgrb.50130>, 2013.

717 Villani, F., Civico, R., Pucci, S., Pizzimenti, L., Nappi, R., De Martini, P. M., and the Open EMERGEO Working Group: A  
718 database of the coseismic effects following the 30 October 2016 Norcia earthquake in Central Italy, *Scientific Data*, 5, 180049,  
719 <https://doi.org/10.1038/sdata.2018.49>, 2018.

720 [Vuan, A., Brondi, P., Sagan, M., Chiaraluca, L., Di Stefano, R., and Michele, M.: Intermittent slip along the Alto Tiberina low](#)  
721 [angle normal fault in central Italy, \*Geophysical Research Letters\*, 47, e2020GL08903, <https://doi.org/10.1029/2020GL089039>,](#)  
722 [2020.](#)

723  
724

## 725 **Data Availability**

726 The downhole logging dataset and additional information about the boreholes are available at the ICDP  
727 repository database (<https://www.icdp-online.org/projects/by-continent/europe/star-italy/public-data/>).

728

## 729 **Author Contributions**

730 Author Contributions: PM, SP, MRB conceptualization, methodology; PM, SP, MTM, AA formal  
731 analysis; PM, SP, MTM, LC, MU, FM, WJ field investigation; LC, AA, MU, FM data curation; PM,  
732 SP, MRB, MTM writing—original draft preparation; SP, MU, MTM visualisation; PM, SP, MRB,  
733 MTM writing—review and editing. All co-authors contributed to reviewing and revising the paper. All  
734 authors have read and agreed to the published version of the manuscript.

## 735 **Competing Interests**

736 The authors declare that they have no conflict of interests.

737 **Acknowledgments**

738 GEOTEC (<http://geo-tec.it/en/>) and GEOLOGIN Srl (<https://www.geolog-in.com/>) are thanked for  
739 providing drillings and geophysical borehole log data. We are grateful to Earthscope for providing  
740 strainmeters. STAR drilling project is co-funded by the International Continental Scientific Drilling  
741 Program (ICDP), by the United States National Science Foundation (NSF) and by the Italian Istituto  
742 Nazionale di Geofisica e Vulcanologia (INGV).

743

744 **Supplementary Material**

745 See Supplementary file